


## RESEARCH ARTICLE

# Analysis of single nuclear chromatin accessibility reveals unique myeloid populations in human pancreatic ductal adenocarcinoma

Hillary G. Pratt<sup>1,2</sup> | Li Ma<sup>3</sup> | Sebastian A. Dziadowicz<sup>3</sup> | Sascha Ott<sup>4</sup> |  
Thomas Whalley<sup>5</sup> | Barbara Szomolay<sup>6</sup> | Timothy D. Eubank<sup>1,2,3,7</sup> |  
Gangqing Hu<sup>2,3</sup> | Brian A. Boone<sup>1,2,3,8</sup> 

<sup>1</sup>Cancer Cell Biology, West Virginia University, Morgantown, West Virginia, USA

<sup>2</sup>WVU Cancer Institute, West Virginia University, Morgantown, West Virginia, USA

<sup>3</sup>Department of Microbiology, Immunology and Cell Biology, West Virginia University, Morgantown, West Virginia, USA

<sup>4</sup>Warwick Medical School, University of Warwick, Coventry, UK

<sup>5</sup>School of Biosciences, Cardiff University, Cardiff, UK

<sup>6</sup>Division of Infection and Immunity & Systems Immunity Research Institute, Cardiff University, Cardiff, UK

<sup>7</sup>In Vivo Multifunctional Magnetic Resonance Center, West Virginia University, Morgantown, West Virginia, USA

<sup>8</sup>Department of Surgery, West Virginia University, Morgantown, West Virginia, USA

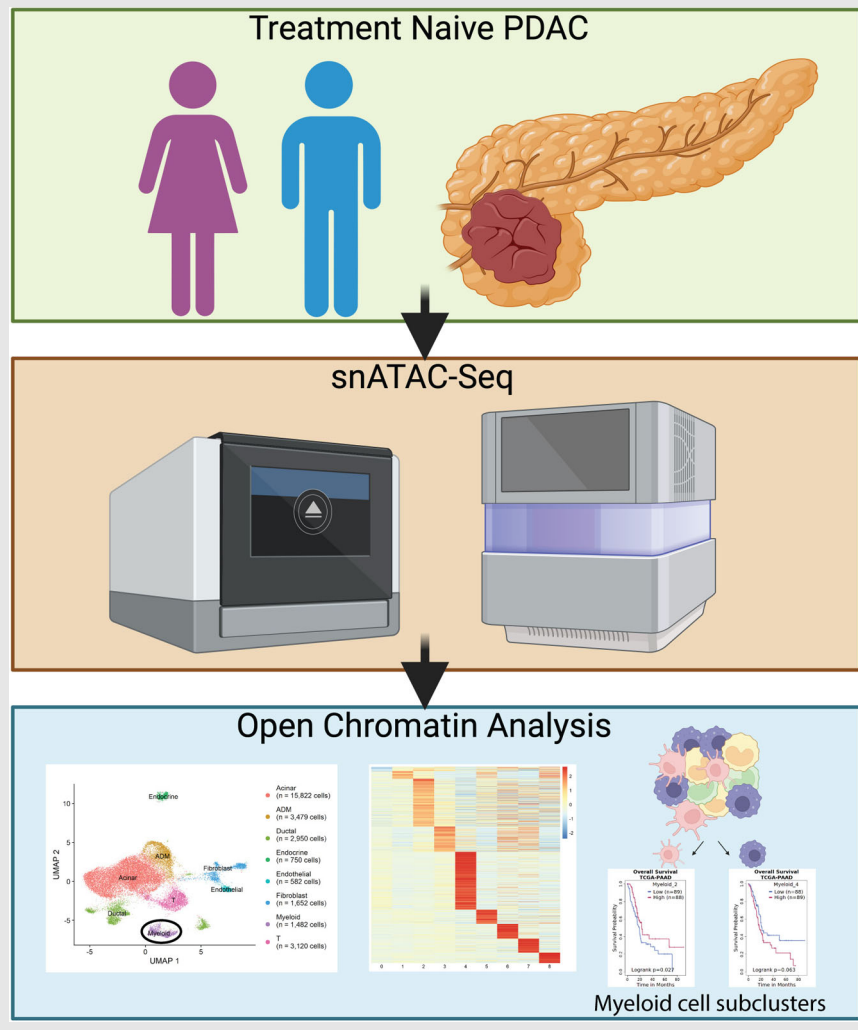
## Correspondence

Brian A. Boone and Timothy D. Eubank, Cancer Cell Biology, West Virginia University, Morgantown, WV, USA. Email: [brian.boone@hsc.wvu.edu](mailto:brian.boone@hsc.wvu.edu), [timothy.eubank@hsc.wvu.edu](mailto:timothy.eubank@hsc.wvu.edu)

Gangqing Hu, WVU Cancer Institute, West Virginia University, Morgantown, West Virginia, USA.

Email: [michael.hu@hsc.wvu.edu](mailto:michael.hu@hsc.wvu.edu)

## Graphical Abstract



1. snATAC-Seq can be used to assay frozen benign pancreatic and PDAC tissues.
2. snATAC-Seq data can be used to determine the regulome and molecular characteristics of cell populations.
3. Myeloid cells from the PDAC TME can be characterized using snATAC-Seq.

## RESEARCH ARTICLE

# Analysis of single nuclear chromatin accessibility reveals unique myeloid populations in human pancreatic ductal adenocarcinoma

Hillary G. Pratt<sup>1,2</sup> | Li Ma<sup>3</sup> | Sebastian A. Dziadowicz<sup>3</sup> | Sascha Ott<sup>4</sup> |  
Thomas Whalley<sup>5</sup> | Barbara Szomolay<sup>6</sup> | Timothy D. Eubank<sup>1,2,3,7</sup> |  
Gangqing Hu<sup>2,3</sup> | Brian A. Boone<sup>1,2,3,8</sup> 

<sup>1</sup>Cancer Cell Biology, West Virginia University, Morgantown, West Virginia, USA

<sup>2</sup>WVU Cancer Institute, West Virginia University, Morgantown, West Virginia, USA

<sup>3</sup>Department of Microbiology, Immunology and Cell Biology, West Virginia University, Morgantown, West Virginia, USA

<sup>4</sup>Warwick Medical School, University of Warwick, Coventry, UK

<sup>5</sup>School of Biosciences, Cardiff University, Cardiff, UK

<sup>6</sup>Division of Infection and Immunity & Systems Immunity Research Institute, Cardiff University, Cardiff, UK

<sup>7</sup>In Vivo Multifunctional Magnetic Resonance Center, West Virginia University, Morgantown, West Virginia, USA

<sup>8</sup>Department of Surgery, West Virginia University, Morgantown, West Virginia, USA

## Correspondence

Brian A. Boone and Timothy D. Eubank,  
Cancer Cell Biology, West Virginia  
University, Morgantown, WV, USA.  
Email: [brian.boone@hsc.wvu.edu](mailto:brian.boone@hsc.wvu.edu),  
[timothy.eubank@hsc.wvu.edu](mailto:timothy.eubank@hsc.wvu.edu)

Gangqing Hu, WVU Cancer Institute,  
West Virginia University, Morgantown,  
West Virginia, USA.  
Email: [michael.hu@hsc.wvu.edu](mailto:michael.hu@hsc.wvu.edu)

## Funding information

National Institute of General Medical  
Sciences of the National Institutes of  
Health (NIH), Grant/Award Numbers:  
U54GM104942, P20GM121322,  
P20GM103434, U54GM104942; NSF MRI,  
Grant/Award Number: 2117043;  
WV-INBRE, Grant/Award Number:  
P20GM103434; COBRE ACCORD,  
Grant/Award Number: 1P20GM121299;

## Abstract

**Background:** A better understanding of the pancreatic ductal adenocarcinoma (PDAC) immune microenvironment is critical to developing new treatments and improving outcomes. Myeloid cells are of particular importance for PDAC progression; however, the presence of heterogenous subsets with different ontogeny and impact, along with some fluidity between them, (infiltrating monocytes vs. tissue-resident macrophages; M1 vs. M2) makes characterisation of myeloid populations challenging. Recent advances in single cell sequencing technology provide tools for characterisation of immune cell infiltrates, and open chromatin provides source and function data for myeloid cells to assist in more comprehensive characterisation. Thus, we explore single nuclear assay for transposase accessible chromatin (ATAC) sequencing (snATAC-Seq), a method to analyse open gene promoters and transcription factor binding, as an important means for discerning the myeloid composition in human PDAC tumours.

**Methods:** Frozen pancreatic tissues (benign or PDAC) were prepared for snATAC-Seq using 10× Chromium technology. Signac was used for preliminary

Hillary G. Pratt and Li Ma contributed equally to this work.

This is an open access article under the terms of the [Creative Commons Attribution](https://creativecommons.org/licenses/by/4.0/) License, which permits use, distribution and reproduction in any medium, provided the original work is properly cited.

© 2024 The Authors. *Clinical and Translational Medicine* published by John Wiley & Sons Australia, Ltd on behalf of Shanghai Institute of Clinical Bioinformatics.

West Virginia Clinical and Translational Science Institute, Grant/Award Numbers: 2U54GM104942, P20GM121322, P20GM144230; National Institute of General Medical Sciences, Grant/Award Numbers: NIGMS 5U54GM104942-04, NIGMS CoBRE 5P20GM121322, NIGMS P20 GM103434, NIGMS P20 GM121322, NIGMS T32 GM133369, NIGMS U54 GM-104942; National Cancer Institute, Grant/Award Numbers: NCI R01CA192064, NCI R01CA194013

analysis, clustering and differentially accessible chromatin region identification. The genes annotated in promoter regions were used for Gene Ontology (GO) enrichment and cell type annotation. Gene signatures were used for survival analysis with The Cancer Genome Atlas (TCGA)-pancreatic adenocarcinoma (PAAD) dataset.

**Results:** Myeloid cell transcription factor activities were higher in tumour than benign pancreatic samples, enabling us to further stratify tumour myeloid populations. Subcluster analysis revealed eight distinct myeloid populations. GO enrichment demonstrated unique functions for myeloid populations, including interleukin-1b signalling (recruited monocytes) and intracellular protein transport (dendritic cells). The identified gene signature for dendritic cells influenced survival (hazard ratio = .63,  $p = .03$ ) in the TCGA-PAAD dataset, which was unique to PDAC.

**Conclusions:** These data suggest snATAC-Seq as a method for analysis of frozen human pancreatic tissues to distinguish myeloid populations. An improved understanding of myeloid cell heterogeneity and function is important for developing new treatment targets in PDAC.

#### KEYWORDS

ATAC-Seq, myeloid, PDAC

## 1 | INTRODUCTION

Although significantly improved over the past decade, the 5-year survival rate for pancreatic ductal adenocarcinoma (PDAC) is only 12%. The unique stromal makeup of the PDAC tumour, including activated fibroblasts and suppressive immune cells, is a critical component driving tumour progression and resistance to therapy. To enhance therapeutic options for PDAC patients, a better understanding of this unique tumour microenvironment (TME) is needed.

Immune cell infiltration of the PDAC TME is an important subject of inquiry as immunotherapies with success in other cancer types have failed in PDAC.<sup>1</sup> In particular, the myeloid component of the PDAC TME has been identified as having a critical role in this immunosuppression and treatment failure. Circulating monocytes were correlated with a worse overall survival in PDAC patients<sup>2</sup>; however, clinical trials blocking monocyte recruitment into the tumour combined with FOLFIRINOX<sup>3</sup> or gemcitabine/nab-paclitaxel<sup>4</sup> demonstrated limited efficacy. Another population of myeloid cells, tissue-resident macrophages (TRMs), are present before tumour initiation and are the prominent source of immunosuppressive, pro-fibrotic macrophages in the PDAC TME in murine models.<sup>5</sup> Meanwhile, M1 and M2

remain the most common characterisation of macrophage populations in the TME, but individual macrophages exist along more of a continuum than this nomenclature reflects.<sup>6</sup> Such studies demonstrate a need for refined characterisation of myeloid source and function in the PDAC TME to understand pathogenesis and uncover novel therapeutic strategies.

Recently, single cell sequencing technologies have been harnessed to determine cell function and composition in the TME. Single cell RNA sequencing (scRNA-Seq) has demonstrated heterogeneity between patients in the tumour and stromal components of PDAC.<sup>7-12</sup> Since stroma can comprise much of the tumour volume,<sup>8,13</sup> scRNA-Seq has been employed to identify the immune cell milieu and ascertain how these cells influence tumour progression,<sup>10</sup> patient prognosis<sup>7,11,12</sup> and chemotherapy response.<sup>11</sup> Given the importance of myeloid cells in PDAC progression,<sup>2,5</sup> scRNA-Seq studies have also explored the phenotype and function<sup>11,12</sup> as well as source,<sup>12</sup> of macrophages. Although the transcriptome of cells within the PDAC TME has been heavily studied,<sup>11,14-16</sup> there has been limited progress on the regulome of cells within the TME. To answer such questions, a method for analysing open chromatin, termed assay for transposase accessible chromatin sequencing (ATAC-Seq), can explore the epigenetic underpinnings of diseases.<sup>17,18</sup> Open chromatin can also be utilised for cell identification due to its role in

regulation of gene expression.<sup>18,19</sup> A limited number of studies exploring single cell chromatin accessibility from freshly isolated PDAC specimens have shown an important role for KRAS regulation of enhancer activity<sup>20</sup> and dysregulation of methylation<sup>7</sup> in PDAC progression, demonstrating the importance of epigenomics in understanding pancreatic diseases. Furthermore, open chromatin and transcription factor activity can be used to determine myeloid cell origin,<sup>19</sup> which is relevant for understanding the highly plastic myeloid populations that are present in the PDAC tumour and the role for these cells in cancer progression.

In the present study, we applied single nuclear ATAC-Seq (snATAC-Seq) to frozen benign and PDAC patient pancreatic specimens. Our results justified snATAC-Seq as an effective method for retrospective analysis of tumours to identify unique cell populations within the TME. Through snATAC-Seq, we combined information on transcription factor binding and gene promoter activity to identify cell populations and infer their functions in benign pancreatic and PDAC samples. Utilising these findings, we then explored the impact of distinct myeloid cell populations on patient survival.

## 2 | MATERIALS AND METHODS

### 2.1 | Patient tissue collection

Prior to sample collection, Institutional Review Board approval was obtained from West Virginia University (#1903496995) and all patients signed informed consent. All patients underwent surgical resection with pancreaticoduodenectomy as part of standard of care. Benign and PDAC samples for snATAC-Seq were treatment naïve. Tissue was obtained from the pathology frozen section suite immediately upon surgical resection. Diagnosis was confirmed by pathology. PDAC tumour tissue or benign pancreatic tissue was frozen alone (nucleus isolation) or in OCT (optimal cutting temperature compound; immunofluorescence staining) and stored at  $-80^{\circ}\text{C}$ .

### 2.2 | Immunofluorescent staining

Sections (10  $\mu\text{m}$ ) of OCT-embedded frozen tissues were fixed in 10% formalin then permeabilised with .1% Triton-X for 10 min and blocked for 1 h at room temperature with 5% bovine serum albumin (BSA; MACS BSA stock solution, Miltenyi Biotec, 130-091-376) and 10% goat serum (Gibco, 16210-072) in Dulecco's Phosphate Buffered Saline (DPBS; Gibco, 14190144). Slides were incubated with

primary antibodies (1:100) overnight at  $4^{\circ}\text{C}$  (mouse anti-human CD11c [Invitrogen, 14-0116-82], mouse anti-human CD11b [Invitrogen, 14-0118-82], rabbit polyclonal SEMA4A [Invitrogen, PA5-101258] and rabbit anti-human TRIM29 [Invitrogen, 703612]). Tissues were incubated with secondary antibody for 1 h at room temperature (Alexa Fluor 488 goat anti-rabbit [Invitrogen, A-11008]; Alexa Fluor 647 goat anti-mouse [Invitrogen, A-21235]). Vector TrueVIEW Autofluorescence Quenching Kit (Vector Laboratories, SP-8400-15) was prepared per manufacturer's instructions and added for 5 min. Then, the slide was stained with DAPI (Thermo Scientific, 62248). Vectashield Vibrance Antifade Mounting Media (Vector Laboratories, H-1700) was used to mount coverslips. All antibodies were diluted in 1% BSA and 10% goat serum in DPBS. Slides were washed with DPBS between steps. Imaging was performed on a Nikon A1R confocal microscope using Nikon A1R software with 60 $\times$  zoom with oil immersion.

### 2.3 | Nuclei isolation from frozen tissue

Isolation procedure was adapted from nuclei isolation from complex tissues for Single Cell Multiome ATAC + Gene Expression Sequencing (CG000375). Nuclei were isolated from 50 mg of frozen tissue cut into five small sections with a razor blade. The tissue pieces were homogenised for 1.5 min with a tissue homogeniser and pestle in 10 mM Tris-HCl, 10 mM NaCl, 3 mM  $\text{MgCl}_2$ , .1% Nonidet P40 substitute and 1 mM dithiothreitol (DTT) in nuclease-free water. Tissue was dissociated in lysis buffer for 5 min before passing through a 70  $\mu\text{m}$  cell strainer. The solution was then centrifuged (500  $\times$  g,  $4^{\circ}\text{C}$ , 5 min). The supernatant was removed and replaced with 1 mL 1% BSA in DPBS and allowed to incubate for 5 min before resuspension. The nuclei were centrifuged again (500  $\times$  g,  $4^{\circ}\text{C}$ , 5 min). The pellet was resuspended in 1 mL 1% BSA in DPBS and passed through a 30  $\mu\text{m}$  cell strainer. All steps were performed on ice. Nuclei were stained with 7-aminoactinomycin D (7-AAD) readymade solution 1:100 (Sigma, SML-1633) and sorted with a FACSaria III Cell Sorter. Nuclei were collected into 10% BSA. For snMultiomics, 1 U/mL RNase inhibitor (Sigma-Aldrich, 03335402001) was added to all final solutions.

### 2.4 | Bulk ATAC-Seq

The Omni-ATAC Protocol<sup>18</sup> was followed. Libraries were prepared with sorted nuclei with a Tagment DNA Enzyme and Buffer Large Kit (Illumina, 20034198) and run on 2% agarose gel to observe the nucleosome phasing pattern and size select. The gel was cut for an approximately

~200–600 bp band and subjected to gel elution using the Qiagen gel MinElute Gel Extraction Kit (Qiagen, 28606).

## 2.5 | snATAC-Seq library preparation

Libraries for snATAC-Seq were prepared as recommended by 10× Genomics using a Chromium Single Cell ATAC Library & Gel Bead Kit (10× Genomics, 1000176). Briefly, sorted nuclei were centrifuged ( $500 \times g$ ,  $4^\circ\text{C}$ , 5 min). The pellet was resuspended in 100 mL  $1\times$  lysis buffer (10 mM Tris-HCl, 10 mM NaCl, 3 mM  $\text{MgCl}_2$ , 1% BSA, 1 mM DTT, .01% Tween-20, .01% Nonidet P40 substitute and .001% digitonin in nuclease-free water) and incubated on ice for 2 min. Nuclei were washed with 1 mL wash buffer (10 mM Tris-HCl, 10 mM NaCl, 3 mM  $\text{MgCl}_2$ , 1% BSA, .1% Tween-20 and 1 mM DTT in nuclease-free water) and centrifuged ( $500 \times g$ ,  $4^\circ\text{C}$ , 5 min). The pellet was resuspended in  $1\times$  nuclei buffer diluted in nuclease-free water. The ATAC reaction was carried out as recommended by 10× Genomics. Nuclei were loaded onto the 10× Chromium Chip E (10× Genomics, 2000171) on the chromium controller to obtain 10 000 nuclei. Library quality was confirmed with an Agilent Bioanalyser. Libraries were sequenced by an Illumina NextSeq 2000 sequencer at Marshall University Genomics Core Facility.

## 2.6 | snMultiome library preparation

Libraries for snMultiome + ATAC were prepared as recommended by 10× Genomics using a Chromium Single Cell Multiome + ATAC Library and Gel Bead Kit (10× Genomics, 1000283). Briefly, sorted nuclei were centrifuged ( $500 \times g$ ,  $4^\circ\text{C}$ , 5 min). The pellet was resuspended in 100 mL  $1\times$  lysis buffer (10 mM Tris-HCl, 10 mM NaCl, 3 mM  $\text{MgCl}_2$ , 1% BSA, 1 U/mL RNase inhibitor, 1 mM DTT, .01% Tween-20, .01% Nonidet P40 substitute and .001% digitonin in nuclease-free water) and incubated on ice for 2 min. Nuclei were washed with 1 mL wash buffer (10 mM Tris-HCl, 10 mM NaCl, 3 mM  $\text{MgCl}_2$ , 1% BSA, 1 U/mL RNase inhibitor, .1% Tween-20 and 1 mM DTT in nuclease-free water) and centrifuged ( $500 \times g$ ,  $4^\circ\text{C}$ , 5 min). The pellet was resuspended in  $1\times$  nuclei buffer with 1 U/mL RNase inhibitor and 1 mM DTT in nuclease-free water. The ATAC and cDNA reactions were carried out as recommended by 10× Genomics. Nuclei were loaded onto the 10× Chromium Chip J (10× Genomics, 1000230) on the chromium controller for 10 000 nuclei. Library quality was confirmed with an Agilent Bioanalyser. Libraries were sequenced by an Illumina NextSeq 2000 sequencer at Marshall University Genomic Core Facility.

## 2.7 | snATAC-Seq data pre-processing and clustering analysis

snATAC-Seq reads were aligned to the GRCH38(hg38) reference genome. Fragment counts were quantified using cellranger-atac count (version 2.1.0). Seurat<sup>21</sup> (version 4.2.1) and Signac<sup>22</sup> (version 1.7.0) were used for downstream analysis. Quality control was based on library features with settings:  $1000 < \text{nCount\_ATAC}$  (number of fragments)  $< 20\ 000$ ,  $500 < \text{nFeature\_ATAC}$  (number of peaks)  $< 10\ 000$ ,  $\text{blacklist\_fraction} < 5\%$ ,  $\text{nucleosome\_signal} < 2$ ,  $\text{TSS.enrichment} > 2$  and  $\text{pct\_reads\_in\_peaks}$  (fraction of fragments within ATAC-Seq peaks)  $> 15\%$ . Nucleosome\_signal (strength of the nucleosome signal), TSS.enrichment (transcription start site [TSS] enrichment score as defined by ENCODE) and blacklist\_fraction (ratio reads in genomic blacklist regions as defined by ENCODE) were calculated by the function NucleosomeSignal, TSSEnrichment and FractionCountsInRegion of Signac, respectively. RunTFIDF was used to compute term-frequency inverse-document-frequency normalisation on the matrix. FindTopFeatures was used to find the most frequently observed features. RunSVD was used to find the top 50 largest singular value and corresponding singular vectors of the matrix. RunHarmony<sup>23</sup> was used to correct batch effects. RunUMAP was used for dimensional reduction and visualisation via uniform manifold approximation and projection (UMAP). FindNeighbours was used to compute the nearest neighbours for the object. FindClusters was used to identify clusters of cells by a shared nearest neighbours modularity optimisation based on Smart Local Moving (SLM) clustering algorithms<sup>24</sup> with a resolution of .2. FindAllMarkers was used to identify the differentially accessible regions for each cluster by against all other clusters, by setting 'LR' as the test used, peak\_region\_fragments as the test variable, and logfc.threshold (fold change in log2 scale) as .25.

## 2.8 | Cell type annotation for the snMultiome dataset

Sequencing reads were aligned to the GRCH38 (hg38) reference genome and quantified using cellranger-arc count (version 2.0.2). Quality control was based on each library's features with these settings:  $500 < \text{nCount\_ATAC} < 40\ 000$ ,  $500 < \text{nCount\_RNA}$  (total number of RNA fragments)  $< 20\ 000$ ,  $100 < \text{nFeature\_ATAC} < 20\ 000$ ,  $100 < \text{nFeature\_RNA}$  (number of genes)  $< 5000$ ,  $\text{nucleosome\_signal} < 2$ ,  $\text{pct\_reads\_in\_peaks} > 15\%$ ,  $\text{percent.mt} < 2\%$ ,  $\text{percent.ribo} < 2\%$ ,  $\text{TSS.enrichment} > 2$  and  $\text{blacklist\_fraction} < 2\%$ . Percent.mt (RNA reads from

mitochondrial genes) and percent.ribo (reads from ribosomal genes) were calculated by the PercentageFeatureSet function.

The RNA part of the snMultiome was used to annotate cell type and the ATAC part for validation of the cell type annotation in the snATAC-Seq (next section). For the RNA part, Seurat<sup>21</sup> (version 4.2.1) was used for downstream analysis. NormalizeData was used for normalisation and set normalisation method as 'CLR' (centered log ratio transformation). Cell cycle phase score was calculated by CellCycleScoring. Variable features were identified by FindVariableFeatures and the top 2000 were selected. Data were scaled and centered by ScaleData function and regress out the cell cycle's effect. RunPCA was used for principal component analysis (PCA) dimensionality reduction. RunHarmony<sup>23</sup> was used to integrate the dataset. RunUMAP and FindNeighbours were called as in the previous section. FindClusters was used to identify clusters of cells by a shared nearest neighbours modularity optimisation based on original Louvain clustering algorithms with a resolution of .2. Cell clusters annotated with marker genes are acinar cell (*CUZD1*<sup>25</sup>), acinar to ductal metaplasia (ADM) cell (*ONECUT1*<sup>26</sup>), ductal cell (*KRT19*<sup>11,15</sup>), endocrine cell (*PAX6*<sup>27</sup>), endothelial cell (*TEK*<sup>28</sup>), fibroblast (*COL1A2*<sup>29</sup>), myeloid cell (*CDI63*,<sup>12</sup> *CSF2RA*<sup>30</sup>) and T cell (*IL7R1*) (Table S1). After annotation, an extended list of marker genes was predicted for each cell type against all other cell types through FindAllMarkers with 'wilcox' test and logfc.threshold as .25 (Table S1).

## 2.9 | Cell type annotation and validation for snATAC-Seq

Cell type annotation for the snATAC-Seq datasets was done through an integrative analysis with annotated cells from the snMultiome dataset. After differential accessible regions were identified for each cluster from the snATAC-Seq dataset (Table S2), promoters overlapping with these peaks were used to define signature genes for each cluster. Signature genes for each cluster from the snATAC-Seq dataset were then compared to marker genes for each cell type defined from the RNA part of the snMultiome data set for an overrepresentation analysis (observed number/expected number) (Figure S5D). For each snATAC-seq cluster, the cell type with the highest overrepresentation was assigned to that cluster.

We validated our snATAC-Seq annotations by four methods (see Section 3). First, expression of representative genes in snATAC-Seq clusters was examined in the snMultiome dataset to visually validate cell type annotation. Second, we identified the overrepresented molecular pathways for snATAC-Seq clusters with Gene Ontology

(GO) enrichment of signature genes. Third, we aligned the snATAC-Seq data with the ATAC part of our snMultiome. Cell type annotation for the ATAC part of the snMultiome data was directly transferred from the RNA part of the snMultiome data. We applied the RunHarmony function in the Harmony package<sup>23</sup> for this alignment, visualised data in UMAP, projected their respective cell type annotation and visually examined their positional relationship.

Lastly, four scATAC-Seq datasets<sup>20</sup> were downloaded from Gene Expression Omnibus (GSE147726) (one patient tumour and adjacent nonmalignant tissue, another tumour and a histologically normal pancreas). While cell types are listed by Li et al.,<sup>20</sup> a file documenting cell annotation is absent from their repository. We therefore reanalysed their data. Briefly, we mapped the raw reads to the hg38 reference genome. Seurat<sup>21</sup> (version 4.2.1) and Signac<sup>22</sup> (version 1.7.0) were used. We identified differential accessible regions of the clusters and signature genes for each cluster through overlapping analysis at promoters. We applied GO enrichment to the signature genes to identify overrepresented pathways for each cluster and used this information to annotate cell types from Li et al.<sup>20</sup> We then used the RunHarmony function in the Harmony package<sup>23</sup> to align our snATAC-Seq datasets with the public scATAC-Seq dataset, visualised cells in UMAP, projected cell type annotation from its respective data set and visually examined the positional relationship.

## 2.10 | Tumour sample snATAC-Seq dataset extraction and annotation

After annotating the benign and tumour snATAC-Seq dataset, we extracted the tumour samples. For this extracted new object, Seurat<sup>21</sup> (version 4.2.1) and Signac<sup>22</sup> (version 1.7.0) were used for downstream analysis. FindClusters was used to identify clusters of cells by a shared nearest neighbours modularity optimisation based on SLM clustering algorithms<sup>24</sup> with a resolution of .8, and we identified 19 subclusters. Each cluster was generally dominated by one cell type after transferring annotation from the benign and tumour samples. Clusters were designated based on the predominant cell type and merged if they shared the same cell type.

To investigate the myeloid subpopulations in PDAC tumours, we extracted the myeloid population (Table S3). Seurat<sup>21</sup> (version 4.2.1) and Signac<sup>22</sup> (version 1.7.0) were used. Myeloid subcluster 0 had no differentially expressed promoters ( $p$ -value < .01) and was identified as a possible myeloid cell transitional state. Myeloid subclusters (>50 nuclei) were annotated—myeloid subcluster 1: recruited monocytes (*ALOX5*,<sup>31</sup> *NLRC4*<sup>32</sup>), myeloid subcluster 2:

dendritic cells (*SEMA4A*,<sup>33,34</sup> *SEMA7A*,<sup>35</sup> *HLA-DRB5*<sup>36,37</sup>), myeloid subcluster 3: myeloid-derived suppressor cells (MDSCs) (*S100A9*, *CSF2RA*, *IFNGR2*)<sup>11,38</sup> and myeloid subcluster 4: tissue resident/epithelial-like macrophages (*KRT7*,<sup>11</sup> *KRT8*,<sup>11</sup> *YAP1*,<sup>5</sup> *COL16A1*<sup>5</sup>).

## 2.11 | ChromVAR analysis of snATAC-Seq dataset

For the snATAC-Seq dataset, RunChromVAR<sup>39</sup> function in Signac<sup>22</sup> (version 1.7.0) was used to calculate the transcription factor enrichment score. Motif matrices were obtained from the JASPAR2020 library. FindAllMarkers was used to identify differentially enriched transcription factor motifs for each subcluster against all other subclusters, 'wilcox' was set as the test used and logfc.threshold was set at .25.

## 2.12 | GO enrichment analysis

Metascape<sup>40</sup> was used for GO enrichment analysis with the complete *Homo sapiens* proteome as background. We selected the top 10 hits for visualisation.

## 2.13 | Survival analysis

The top 10 genes (by *p*-value) specific to a myeloid subcluster identified from differential accessibility analysis were used for survival analysis in the Survival Genie application.<sup>41</sup> The Survival Genie Analysis Type selection criteria were 'Gene-Based', 'GENE SETS' and 'Upload my own'. Additional settings were select program: 'TCGA', select dataset: 'TCGA-PAAD, TCGA-CHOL, TCGA-COAD or TCGA-STAD', select tumour: 'Primary', select groups: 'Median', select survival: 'Overall Survival', select tumor infiltrating lymphocytes (TILS): LM22. The survival curves, hazard ratios and *p*-values are reported.

# 3 | RESULTS

## 3.1 | Single nuclear analysis of open chromatin shows unique cell populations in benign pancreas and PDAC

Benign pancreatic ( $n = 4$ ) and PDAC ( $n = 4$ ) samples were obtained following pancreaticoduodenectomy for eight total patients. Patients had pathology in the pancreatic head, which represents the majority of PDAC cases,<sup>42</sup> and had no neoadjuvant chemotherapy, as neoadjuvant therapy may modulate myeloid cell populations.<sup>2,11,43</sup> Patients

were of similar sex and age, and pathology was confirmed by histopathology of the resected specimen listed in Figures S1 and S2. Single nuclei suspensions were made directly from frozen tissues. Debris and ruptured nuclei were removed via fluorescence activated cell sorting (FACS), and we tested the transposase reaction for ATAC-Seq to identify a nucleosome banding pattern (Figure S3). After determining the method preserved chromatin integrity, we proceeded with chromatin accessibility in single nuclei. Combining benign and tumour samples into one UMAP, we showed similarity in the benign pancreatic samples but heterogeneity between PDAC projections (Figure 1A) and characteristic of PDAC tumours.<sup>9,11,15</sup> While there was some overlap in projections between nuclei from benign specimens and PDAC, the benign and tumour samples generally separated, with 18 694 nuclei identified for the benign specimens and 11 143 nuclei identified for the PDAC specimens (Figure 1B). We annotated eight cell clusters in the benign and tumour combined UMAP through an integrative analysis with the RNA part of snMultiome data for tumour and adjacent control tissues collected from an additional patient (Figures S4–S6), of which the cluster were annotated by expression of literature-supported markers (Figure S4). Marker genes of each snATAC-Seq cluster were predicted based on differential promoter openness (Figure S5B; see Table S2 for a full list of the predicted markers). For each snATAC-Seq cluster, we annotated each cell type by cross-referring its open chromatin markers to RNA markers for each cell type identified from snMultiome RNA data, calculated over-representations, and used that information to transfer the cell annotation at cluster level (Figure S5C). Representative marker genes from each of the snATAC-Seq clusters were then validated by gene expression in the snMultiome RNA data (Figure S5D). We further validated the annotation through inspecting the positional relationship of the clusters from the snMultiome ATAC when aligned with those from the snATAC-Seq dataset (Figure S6). Similarly, we validated the annotation with a published scATAC-Seq dataset derived from freshly acquired nuclei suspensions (Figure S7).<sup>20</sup>

The annotations for the snATAC-Seq data are summarised in Figure 1C. The majority of nuclei (53.0%) clustered into the acinar cell group (Figure 1D), aligning with literature showing acinar cells constitute approximately 50% of cells in healthy pancreas. Benign samples are predominated by acinar and ADM cells, while myeloid cells are specific to tumour samples (Figure 1E,F). We conducted a Fisher's exact test on the count of each cell type in both benign and tumour samples, yielding *p*-values consistently less than 5.3e-25. These findings show the unique cellular composition of the PDAC TME compared to benign pancreas identified by snATAC-Seq.



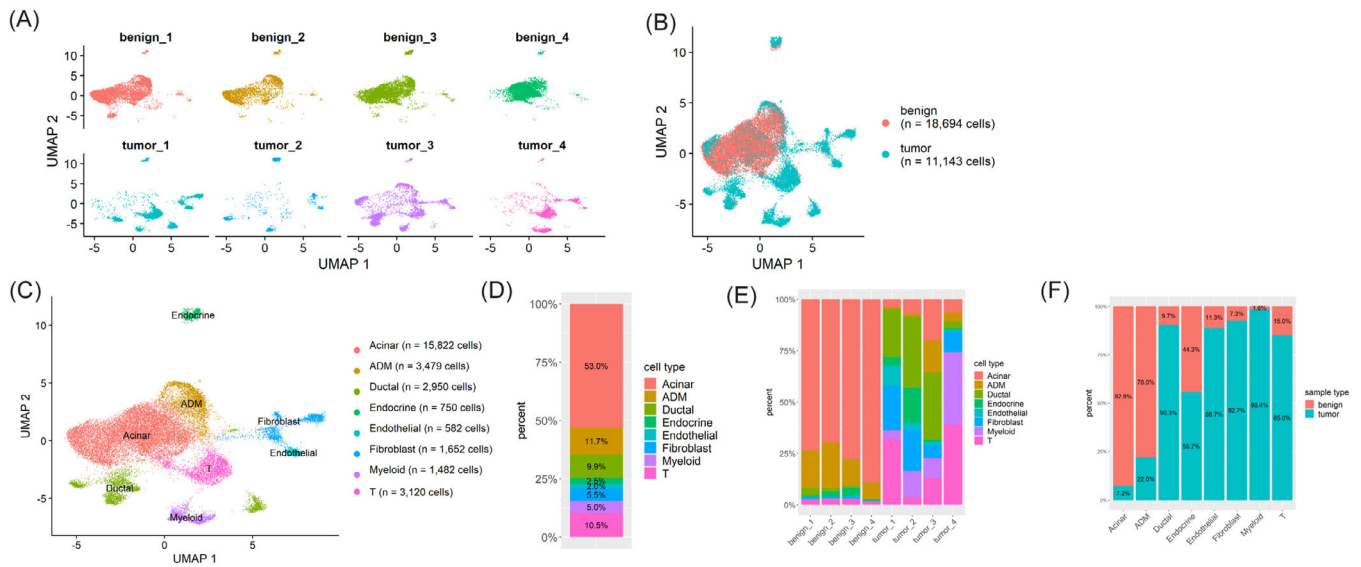


**FIGURE 1** Cellular heterogeneity and unique cell population to pancreatic adenocarcinoma (PDAC). (A) Uniform manifold approximation and projection (UMAP) visualisation of benign and PDAC single nuclear assay for transposase accessible chromatin (ATAC) sequencing (snATAC-Seq) dataset. (B) UMAP visualisation comparing benign and PDAC. (C) UMAP visualisation of the cell clusters and their annotations. (D) Cell type distribution among benign and PDAC snATAC-Seq datasets. (E) Cell type distribution among each dataset of benign and PDAC samples, highlighting myeloid (purple) as a unique cell population presented in PDAC samples. (F) Cell distribution comparing benign and tumour contribution to cell types.

### 3.2 | Open chromatin provides insight into the regulome and cellular function in benign and PDAC specimens

Chromatin accessibility can be used to infer transcription factor activity, gene promoter activity and therefore predicted molecular functions. Utilising chromVAR,<sup>39</sup> we identified differential binding of transcription factors across cell clusters (Figure 2A). In this analysis, acinar cells were enriched with T-cell factor/lymphoid enhancer factor 3 and 12 (TCF3 and TCF12) and Nuclear Receptor Subfamily 5 Group A Member 2 (NR5A2), transcription factors responsible for development and maintenance of the exocrine pancreas.<sup>45</sup> In the ADM cluster, members of the TEA domain (TEAD) transcription factor family (TEAD1–4) have increased activity compared to the acinar cluster. TEAD transcription factors target SRY-Box Transcription Factor 9 (SOX9),<sup>46</sup> which drives ADM.<sup>26</sup> The ductal cell transcription factor activity was primarily driven by malignant ductal cells characterised by FOS/JUN activity, which comprise the activator protein 1 (AP-1) transcription factor<sup>47</sup> and have been implicated in PDAC development.<sup>48</sup> Endocrine cell transcription factor activity was characterised by the regulatory factor X (RFX) transcription factor, important for development and maintenance of pancreatic beta cell function.<sup>49</sup> Endothelial cell development is driven through ETS (E26 transformation specific) and ETV (ETS variant) transcription factors<sup>50</sup> also supported from the ChromVAR analysis. The fibroblast cluster

showed activation of SMAD2/3 transcription factor activity, which is important for cancer-associated fibroblasts development and gemcitabine resistance in PDAC.<sup>51</sup> The T cell cluster was also characterised by ETS transcription factors 1 and 2. ETS1 and ETS2 have differential functions in human T cells. ETS1 is high in resting T cells, while ETS2 mRNA and protein increase after T-cell activation.<sup>52</sup> Transcription factor SPI1 is elevated in the myeloid subset as this is the primary transcription factor driving myeloid lineage cells and promotes monoopoiesis over granulopoiesis and lymphoid cell development.<sup>53</sup> Overall, ChromVAR analysis provides important transcription factor activity data consistent with cell type annotations, again confirming the validity of our cell type annotation for the snATAC-Seq data sets.

Next, we focused on genes with promoters preferentially opened in one cell type (Table S2). The promoter openings of those genes were first visualised using heatmap (Figure 2B). We next focused on promoter openings at genes known to be markers for each cell type (Figure 2C): regenerating family member 1 alpha (*REG1A*) is expressed by acinar cells.<sup>11</sup> The ADM group was characterised by transient receptor potential vanilloid member 6 (*TRPV6*) promoter opening, implicated in promoting pancreatic cancer.<sup>54</sup> Ductal cells in PDAC are characterised as keratin 19 (*KRT19*) positive.<sup>11,15</sup> Endocrine cells have openings at the promoter for Paired box 6 (*PAX6*), important for development and maintenance of the endocrine pancreas in murine models.<sup>27</sup> Promoter opening at the platelet

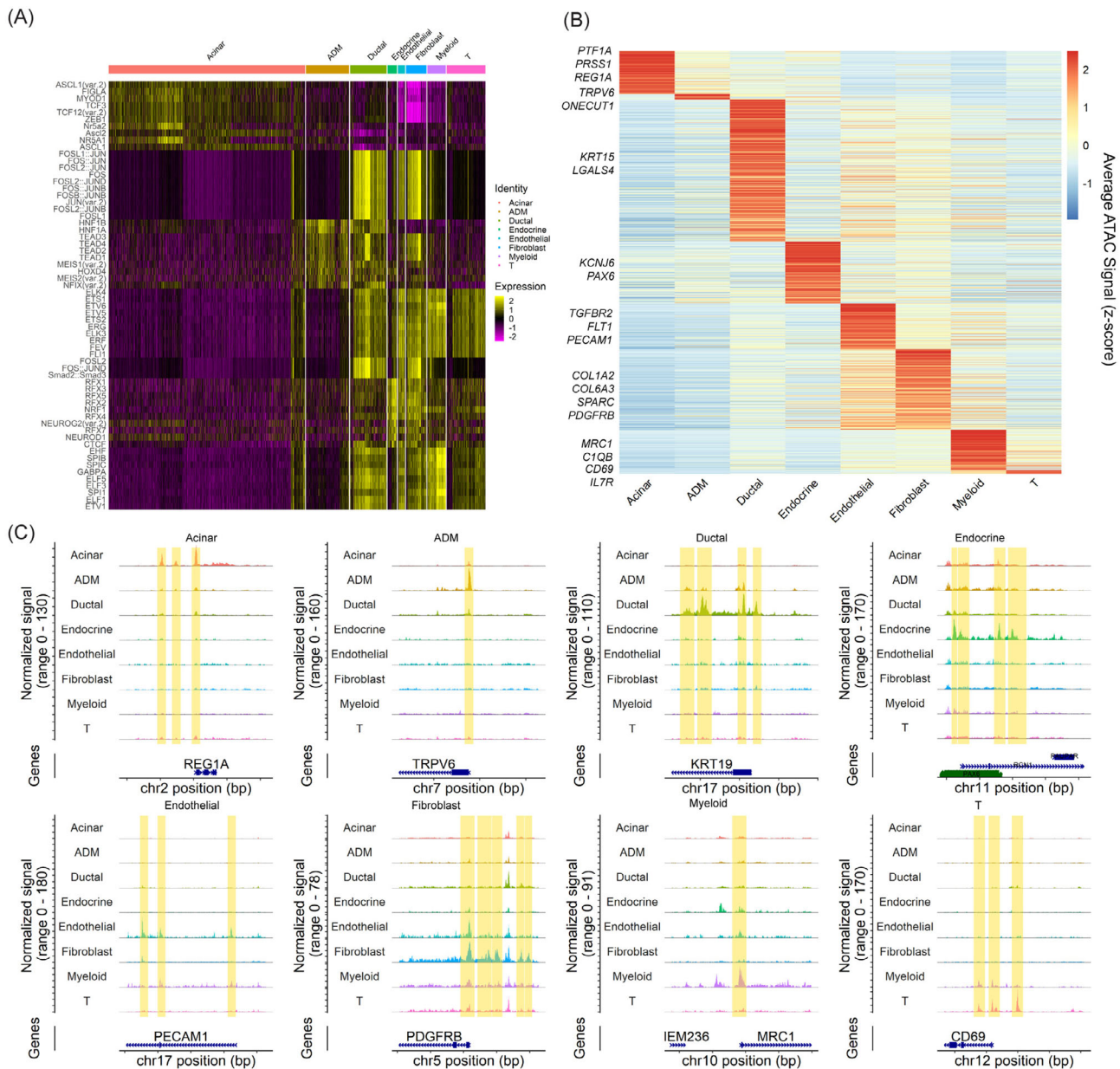


**FIGURE 2** Regulome and molecular characterisation of cell populations identified in benign and pancreatic adenocarcinoma (PDAC) single nuclear assay for transposase accessible chromatin (ATAC) sequencing (snATAC-Seq) datasets. (A) Heatmap of top enriched transcription factor motifs activity (row) across cells organised into annotated clusters (column). (B) Heatmap of the ATAC signal at promoters of genes showing cluster-specific chromatin accessibility. The signal was averaged across all cells within each cluster. Represented genes were shown on the left. (C) Genome browser tracks for ATAC signal across representative genes of each cell type (shown at the top) with differentially accessible regions (including the promoters) highlighted by orange strips. (D) Gene Ontology (GO) enrichment analysis results for genes with promoters differentially accessible in benign samples as compared to tumour samples. (E) GO enrichment analysis results of genes with promoters differentially accessible in PDAC tumour samples as compared to benign. (F) GO enrichment analysis results for genes with promoter specifically accessible in designated cell types (shown at the top) as compared to all others. GO enrichment  $p$ -value is indicated by bar color with scale showing the  $-\log p$ -value to the right. nGenes represents the number of genes under this GO term.

and endothelial adhesion molecule 1 (*PECAM1*) promoter is characteristic of endothelial cells.<sup>11</sup> Platelet-derived growth factor receptor beta (*PDGFRB*) is characteristic of PDAC fibroblasts.<sup>15</sup> The myeloid population had opening at the Mannose receptor C-type 1 (*MRC1*) gene, characteristic of suppressive macrophages prevalent in PDAC.<sup>5,12</sup> The

T-cell population was characterised by promoter opening at *CD69*, an early activation marker for T cells expressed by T cells in PDAC.<sup>55</sup>

Then, we performed GO enrichment using the genes to identify unique molecular functions between the benign pancreas and PDAC. In the benign specimens, the

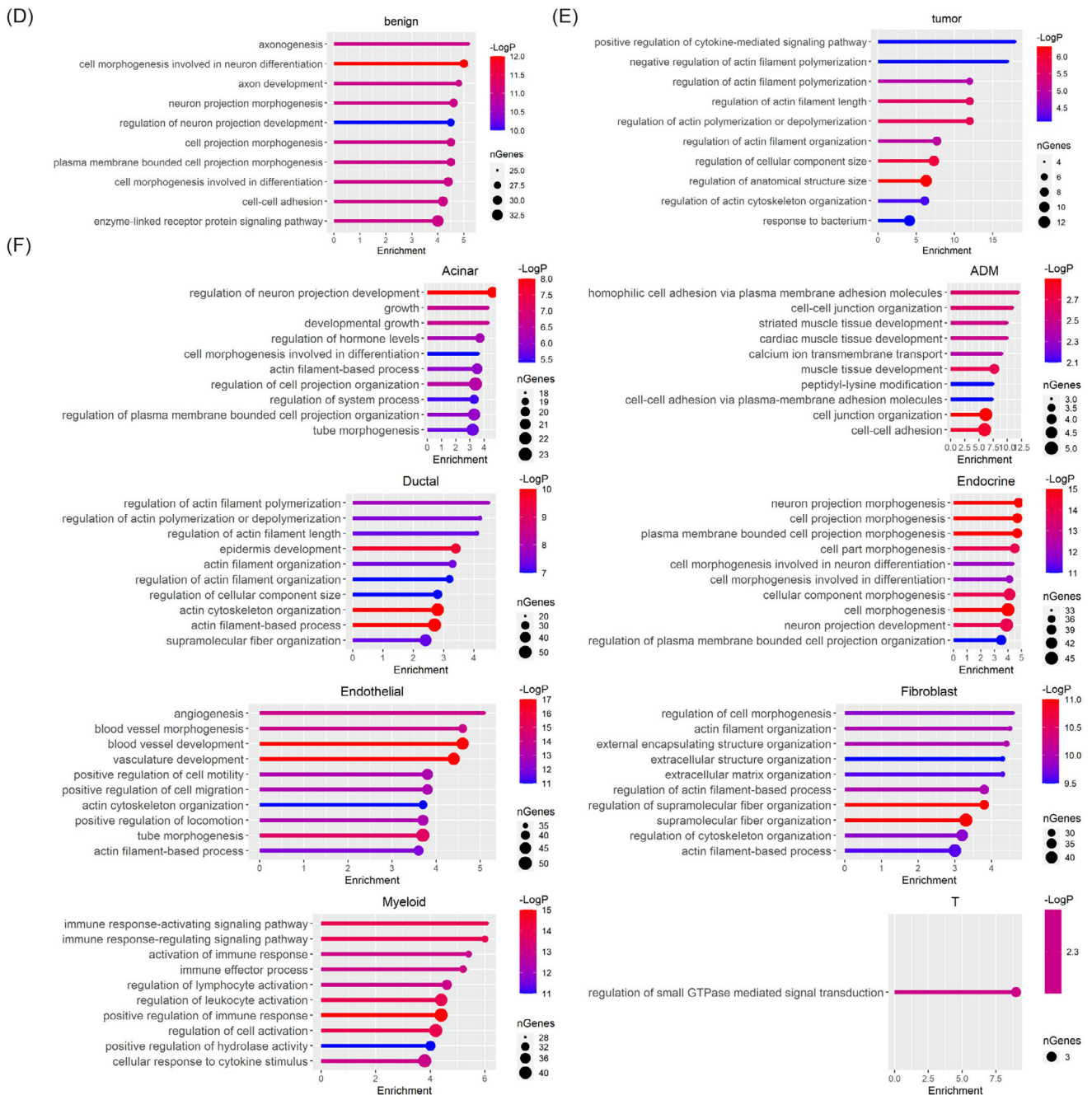


FIGURE 2 Continued

GO enrichment was predominantly related to the nervous system, including axonogenesis, cell morphogenesis involved in neuron differentiation and axon development (Figure 2D), similar to previous analysis.<sup>7</sup> These findings demonstrate the strong link between the nervous system and both the endocrine (alpha, beta and delta cells) and exocrine (acinar and ductal cells) pancreas, which are under control of the autonomic nervous system.<sup>56</sup> In PDAC specimens, the hallmarks of the nervous system-pancreas crosstalk are replaced with functional terms for inflammation (positive regulation of cytokine-mediated signalling

pathway), confirming previous scRNA-Seq analyses<sup>15</sup> and regulation of actin filament length, indicative of migratory or dividing cells (Figure 2E).<sup>57</sup> Previous studies have also shown similar dysregulation of axonal guidance pathways in the progression to PDAC.<sup>7</sup>

We further applied GO enrichment to identify overrepresented molecular pathways in each cluster (Figure 2F; full list is provided in Table S4). Analysis of the acinar cell and endocrine clusters reveals the connection between the autonomic nervous system and pancreas for normal pancreatic development and function.<sup>56</sup> The acinar cell cluster

GO enrichment of regulation of neuron projection development contains the gene *GFII*, which is known for its function in development of acinar cells.<sup>58</sup> Furthermore, *FGF9* and *FGF10*, genes recently shown to be involved in pancreatic development<sup>59</sup> and previously known to be important for neuronal development and maturation<sup>60</sup> play a role in the GO pathway developmental growth for the acinar cell cluster. In the endocrine cluster, the GO pathway neuron projection morphogenesis is characterised by *Pax6*, a gene responsible for development of the pancreas and other neuroectodermal structures,<sup>61</sup> *ISL1*, a gene important for beta cell function,<sup>62</sup> and *ITGB1*, a gene coding for an integrin critical for islet cell development in the pancreas<sup>63</sup> and for neuronal cell migration.<sup>64</sup> ADM GO enrichment includes cell–cell junctions and adhesions, representing the transition of acinar cells to a more ductal-like phenotype.<sup>15</sup> In the ADM GO enrichment, *PCDH1*, a negative prognostic indicator in PDAC<sup>65,66</sup> is one of the genes for homophilic cell adhesion via plasma membrane adhesion molecules. Also, interestingly, the gene *HEGL1*, which codes for a membrane protein that may be targeted in mesothelioma,<sup>67</sup> plays a role in the GO enrichment for cell–cell junction organisation. The ductal cells, which were primarily composed of tumour cells, have GO enrichment related to actin filaments.<sup>57</sup> Specifically, the genes *CAPG*<sup>68</sup> and *VASP*,<sup>69</sup> which are related to metastasis in gastrointestinal cancers are represented in the regulation of actin polymerisation GO biological process identified as a function of the ductal cells. The endothelial cells function in blood vessel and vasculature development. In the endothelial cell cluster, the angiogenesis GO pathway was characterised by genes *NOS3*, important in VEGF-induced angiogenesis<sup>70</sup> and implicated as a therapeutic target in PDAC,<sup>71</sup> and *FGF1*, a known inducer of angiogenesis.<sup>72</sup> The fibroblast cluster showed expected functions of extracellular matrix and structure organisation,<sup>11</sup> which were characterised by collagen genes (*COL1A2*, *COL5A1*, *COL8A1*, *COL16A1*). Interestingly, the fibroblast GO enrichment showed functions of regulating cell morphogenesis. Cancer-associated fibroblasts can activate epithelial to mesenchymal transition (EMT) in pancreatic cancer,<sup>73</sup> and the fibroblast GO biological pathway was also characterised by *SPARC* expression, which promotes tumour cell invasiveness in triple negative breast cancer when released by fibroblasts.<sup>74</sup> As previously shown,<sup>75</sup> T cell activation involves regulation of GTPase mediated signal transduction. The gene *ARHGAP15* was involved in the GO biological process for T cells, and previous studies have shown that different isoforms of ARHGAP15 may play different roles in T cell activation.<sup>76</sup> For the myeloid cluster GO enrichment, activation of immune response was characterised by the inflammasomes (*NLRP1*, *NLRP3* and *AIM2*), which can

activate inflammation in myeloid cells<sup>77</sup> but may cause immunosuppressive T cells in PDAC.<sup>78</sup> This function of myeloid activation of the immune system may be contrary to previous reports of myeloid cells in PDAC having immunosuppressive effects.<sup>2,79</sup> Interestingly, the myeloid GO biological process, cellular response to cytokine stimulus, was characterised by genes *MRC1* and *CSF2RA*, which are commonly associated with more immunosuppressive phenotypes in myeloid cells,<sup>5,11,12,38</sup> demonstrating that the myeloid cells responding to cytokine stimuli may be reprogrammed to an immunosuppressive phenotype. These findings suggest a spectrum of myeloid effector states in the PDAC TME, which should be further stratified. Taken together, these findings represent snATAC-Seq as a powerful tool for cellular heterogeneity delineation, regulome characterisation and molecular function inference from frozen pancreatic tissue.

### 3.3 | High myeloid cell activity is characteristic of PDAC tumours but does not predict patient survival

Given the importance of myeloid cells in PDAC and inherent challenges with characterising these highly plastic cells, we next sought to determine if snATAC-Seq could give insight into myeloid cells. First, we determined that ChromVAR-inferred binding of transcription factors important for driving myeloid cell development (such as SPI1 and CEBPA) were more significantly more prevalent in tumour than benign pancreata (Figures 3A,B). These data further demonstrate the findings in Figure 1, in which only 24 nuclei representing myeloid cells (1.6% of the total myeloid population) were identified in the benign pancreata, consistent with previous analyses showing limited myeloid cells in normal pancreas.<sup>12,20</sup> Given, the low number of myeloid nuclei identified in the benign pancreata, we further characterised the myeloid subpopulations in the PDAC TME alone. To do this, we re-clustered only the PDAC samples and annotated all the cell populations. We then focused on myeloid cells in the tumour samples (Figure 3C) and identified the top 10 genes with differential promoter openings in this cluster relative to other clusters (Figure 3D). Stratifying patients by high or low myeloid gene signatures using the Survival Genie application with the pancreatic adenocarcinoma (PAAD) dataset from The Cancer Genome Atlas (TCGA), we found no difference in overall survival between patient populations based on high or low expression of the tumour myeloid cell gene signature (Figure 3D). Since previous studies showed differences in disease progression or patient prognosis based on myeloid subsets in the tumour,<sup>2,5,9,79</sup> we next sought to stratify the myeloid cells.

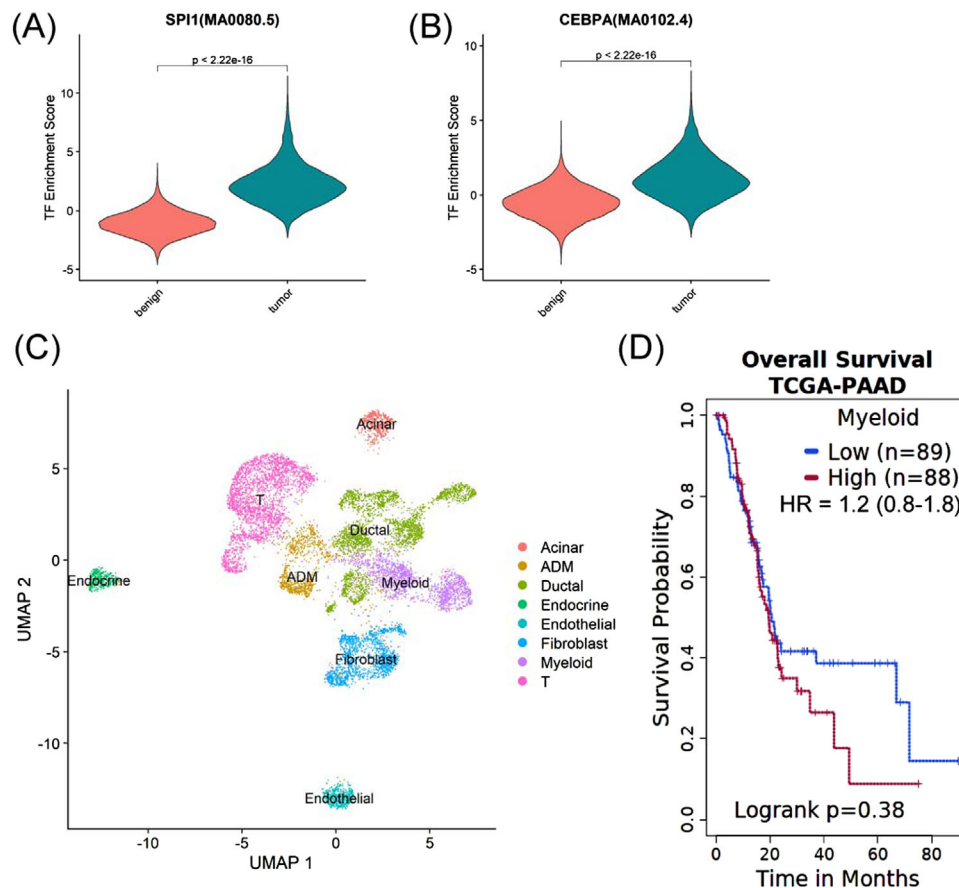


**FIGURE 3** Myeloid populations are higher in pancreatic adenocarcinoma (PDAC) tumour than benign pancreas. (A) Violin plot for transcription factor activity corresponding to SPI1 motif for benign and PDAC tumours from ChromVAR analysis on single nuclear assay for transposase accessible chromatin (ATAC) sequencing (snATAC-Seq) data. The mean comparison p-value was calculated with wilcox.test method. (B) Violin plot for CEBPA motif. (C) Re-clustering and uniform manifold approximation and projection (UMAP) visualisation of cell type among PDAC tumours datasets. (D) Kaplan–Meier survival curve for ‘The Cancer Genome Atlas (TCGA)-pancreatic adenocarcinoma (PAAD)’ patients sorted by overall expression of myeloid signature genes identified from snATAC-Seq analysis.

### 3.4 | Unique myeloid cell populations exist in PDAC tumour and have distinct functions

Observing no survival difference between groups with high and low myeloid signature gene expression, we further delineated the myeloid cluster into subclusters corresponding to several types of myeloid cells.<sup>11</sup> We extracted the myeloid cell populations from the PDAC tumour samples (Figure 4A), performed re-clustering analysis and identified nine subclusters (Figure 4B). Most cells grouped into subclusters 0–4, which had contributions from all the assayed tumours (Figure 4B). The four smaller clusters of nuclei (subclusters 5–8) comprising less than 50 nuclei each and not represented in all tumours were excluded from further analysis (Figure 4B). Our snATAC-Seq analysis revealed each patient contributed differently to each myeloid subcluster (Figure 4C) consistent with the concept of tumour immune cell heterogeneity.<sup>9,11</sup> Overall, analy-

sis of myeloid cell populations from frozen PDAC tumours identified five major myeloid cell populations for further analysis type and function.

To further characterise the myeloid subpopulations, we determined their unique promoter openings, transcription factor activity and functional profiles. We first identified promoter regions preferentially open in each subcluster (Figure 5A). We noted no promoter upregulation in subcluster 0, suggesting the cells might be in a transitional state. In myeloid subcluster 1, we identified promoters for monocyte-related genes (*ALOX5* and *NLR4*). Arachidonate 5-lipoxygenase (*ALOX5*) is important for generating leukotrienes from arachidonic acid,<sup>31</sup> while NLR family CARD domain containing 4 (*NLR4*) is a monocyte marker<sup>32</sup> important for activation of the innate immune response.<sup>80</sup> Myeloid subcluster 2 is characterised by semaphorin 4A (*SEMA4A*), a marker for dendritic cell activation of T cells,<sup>33,34</sup> and semaphorin 7A (*SEMA7A*), which promotes dendritic cell migration.<sup>35</sup> Myeloid

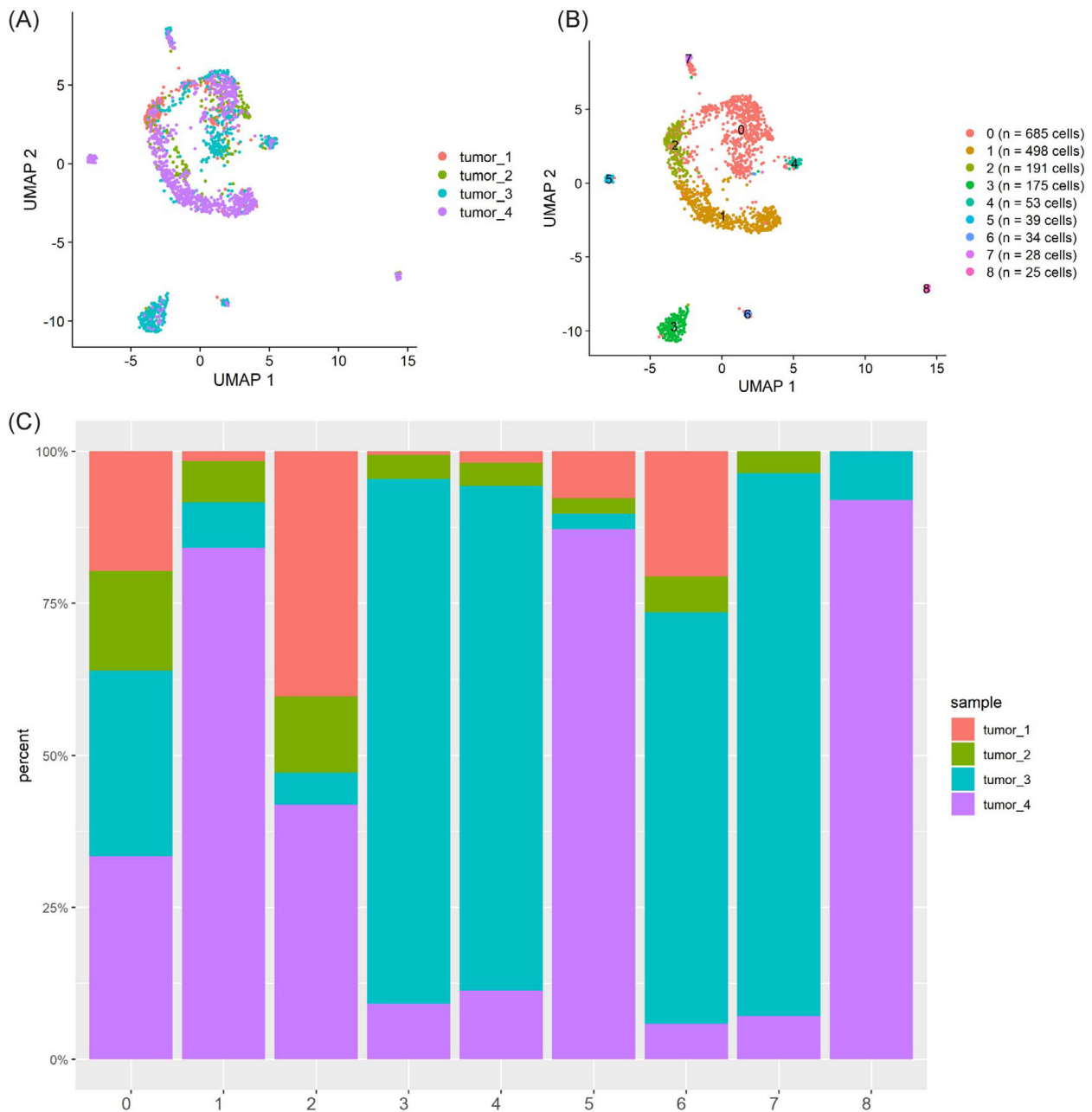


**FIGURE 4** Myeloid subclusters in pancreatic adenocarcinoma (PDAC) tumours. (A) Uniform manifold approximation and projection (UMAP) visualisation of the PDAC tumour dataset only for the myeloid populations. (B) UMAP visualisation of the identified subclusters. (C) Distribution of cells from each PDAC tumour to the subclusters identified in (B).

subcluster 3 was identified as MDSCs based on S100 calcium binding protein A9 (*S100A9*), colony stimulating factor 2 receptor subunit alpha (*CSF2RA*) and interferon gamma receptor 2 (*IFNGR2*) expression.<sup>11,38</sup> Myeloid subcluster 4 was characterised by collagen expression (*COL16A1*, *COL4A3*, *COL22A1*, *COL18A1*) and Yes1-associated transcription regulator (*YAP1*), all TRM markers in murine PDAC.<sup>5</sup> Myeloid subcluster 4 also expresses keratin 7 and 8 (*KRT7* and *KRT8*) aligning with epithelial-like myeloid cells identified by scRNA-Seq in PDAC.<sup>11</sup>

ChromVAR analysis of the transcription factor activity between the myeloid clusters was mostly distinct with some overlap as expected from highly plastic myeloid populations (Figures 5B,C). Myeloid subcluster 0 is characterised by FOXO transcription factor activity, which is important in maintenance of haematopoietic stem cells<sup>81</sup> and may be important in peritoneal TRMs.<sup>82</sup> These cells may be a transitional state of myeloid cell as pancreatic TRMs can be replaced by stem cells upon damage to the pancreas.<sup>83</sup> Myeloid subclusters 1 (recruited monocytes) and 2 (dendritic cells) were characterised by IRF1

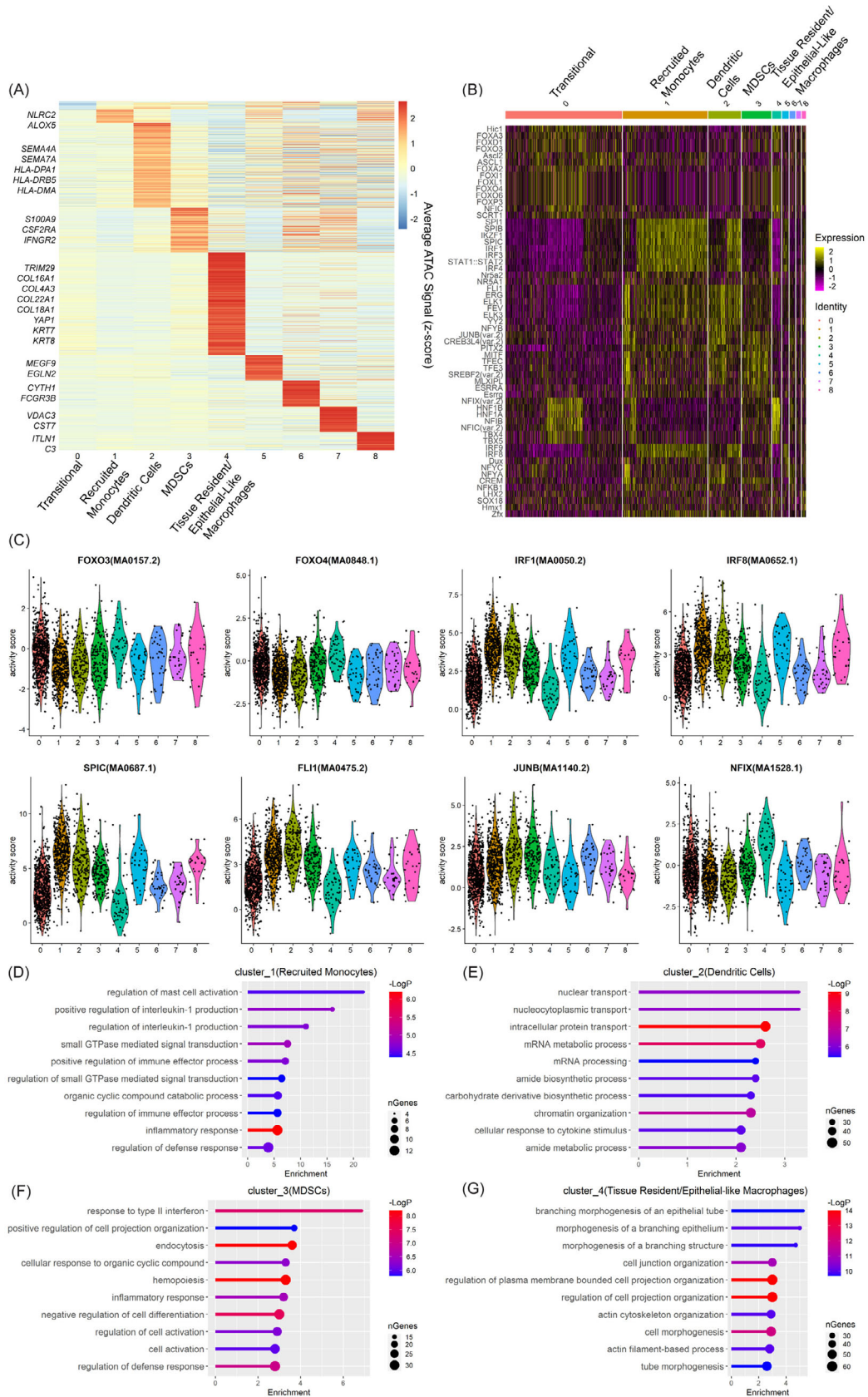


**FIGURE 5** Characterisation of myeloid subclusters in pancreatic adenocarcinoma (PDAC) tumours. (A) Heatmap of the assay for transposase accessible chromatin (ATAC) signal at promoters showing cluster-specific chromatin accessibility within the myeloid subclusters. The signal was averaged across all cells within each subcluster. Represented genes were shown on the left ( $p < .01$ ). (B) Heatmap of top

transcription factor activity, a promoter of anti-tumour immunity in conventional dendritic cells.<sup>84</sup> IRF8 binding is also higher in myeloid subclusters 1 (recruited monocytes) and 2 (dendritic cells) and promotes differentiation of monocytes and dendritic cells.<sup>85,86</sup> In myeloid subcluster 1 (recruited monocytes), the SPIC transcription factor, promoting anti-inflammatory function in monocytes<sup>87</sup> and angiogenic tumour-associated macrophages,<sup>88</sup> is characteristic. In contrast, FLII transcription factor in myeloid subcluster 2 (dendritic cells) is elevated, which drives development of phagocytic monocytes in mice.<sup>89</sup> Myeloid subcluster 3 (MDSCs) has higher JunB and lower IRF8 activity. While JunB can drive macrophage activation,<sup>90</sup> it also drives MDSCs.<sup>91</sup> IRF8 activity, which suppresses MDSC development, is lower in myeloid subcluster 3 (MDSCs).<sup>92</sup> The transcription factor activity for myeloid subcluster 4 (tissue resident/epithelial-like macrophages) is similar to the activity for ADM, resembling the epithelial-like myeloid cells shown by scRNA-Seq in PDAC.<sup>11</sup> Myeloid subcluster 4 also has elevated FOXO4 activity, whose activity has been shown to downregulate genes in peritoneal TRMs after feeding.<sup>82</sup> Furthermore, NFIX, elevated in myeloid subcluster 4 (tissue resident/epithelial-like macrophages), can drive fibrosis in macrophages in murine models of muscular dystrophy.<sup>93</sup> Taken together, these findings give insight into specific regulome of each myeloid subset.

We next performed GO enrichment analysis to understand the molecular function of the myeloid cells (Table S5). We show that recruited monocyte (myeloid subcluster 1) function is related to mast cell activation (*IL4R*, *NECTIN2*), IL-1b production (*TYROBP*, *NLRP3*) and positive regulation of immune effector processes (*IL1B*, *IL4R*, *NLRP3*) (Figure 5D), suggesting monocytes are recruited and activated. Dendritic cell (myeloid subcluster 2) activity was related to nuclear, nucleocytoplasmic and intracellular transport (*BCL3*, *STAT3*, *CBLB*) (Figure 5E), related to the function of dendritic cell antigen processing and presentation.<sup>94</sup> MDSC (myeloid subcluster 3) GO enrichment showed response to type II interferon (*IFNGR*, *CXCL16*, *IRF1*, *TLR2*) (Figure 5F). Type II interferon response is linked to recruited monocytes<sup>95</sup> and MDSCs.<sup>38</sup> Tissue resident/epithelial-like macrophage (myeloid subcluster 4) activity demonstrated actin cytoskeletal organisation (*ACTG1*, *ACTN1*, *MYOIF*, *MYOIA*, *MYOIC*) (Figure 5G), which may indicate cell division characteristic of TRMs in PDAC murine models<sup>5</sup> and exacerbated

with chemotherapy.<sup>43</sup> Overall, our refined snATAC-Seq analysis delineated cellular heterogeneity among myeloid cells in PDAC tumours and identified molecular pathways overrepresented in each subpopulation.

### 3.5 | Genotypic signatures of dendritic cells and tissue-resident macrophages may predict survival in PDAC patients

Having annotated the identity and functions of the myeloid subclusters, we next endeavored to determine if these myeloid subpopulations impacted survival. To assess a large patient cohort, we explored gene signatures for myeloid subpopulations in the TCGA-PAAD dataset. Using the Survival Genie<sup>41</sup> application, the signature genes for myeloid subcluster 1 (recruited monocytes) showed no survival difference, likely due to the mixed nature of this subset, where classical (pro-inflammatory) and nonclassical (anti-inflammatory) monocytes may have disparate effects on survival (Figure 6A). In contrast, high expression of the myeloid subcluster 2 (dendritic cell) signature in the tumour improved patient survival in the TCGA-PAAD cohort (Figure 6B), which has been similarly reported for circulating dendritic cells.<sup>36</sup> We demonstrate no difference in survival based on the myeloid subcluster 3 (MDSC) gene signature (Figure 6C). While not statistically significant in the TCGA-PAAD cohort, there is a trend ( $p = .063$ ) towards improved survival in patients with lower gene signature for myeloid subcluster 4 (tissue resident/epithelial-like macrophages) (Figure 6D). We then compared the significant gene signatures for myeloid subclusters 2 (dendritic cells) and 4 (tissue resident/epithelial-like macrophages) in other gastrointestinal malignancies, including colon adenocarcinoma (TCGA-COAD), cholangiocarcinoma (TCGA-CHOL) and stomach adenocarcinoma (TCGA-STAD) and saw no significant differences in survival (Figure S8). These findings support previous findings demonstrating that the prognostic significance of the myeloid cell infiltrate is unique to PDAC.<sup>11</sup>

Since we identified significant improvement in survival for the cluster 2 signature (dendritic cells) and a trend towards significant detriment to survival for the cluster 4 signature (tissue resident/epithelial-like macrophages) in the TCGA-PAAD dataset, we performed fluorescent immunohistochemistry to qualitatively identify co-staining of signature genes that may be important for the

---

enriched transcription factor motifs activity (row) across cells organised into subclusters from myeloid cells (column). (C) The violin plot showing ChromVAR-inferred transcription factor activity score for selected motifs across subclusters. (D–G) Gene Ontology (GO) enrichment analysis results for genes with promoters preferentially open in myeloid subcluster of 1 (D), 2 (E), 3 (F) and 4 (G). GO enrichment  $p$ -value is indicated by bar color with scale showing the  $-\log p$ -value to the right. nGenes represents the number of genes under this GO term.



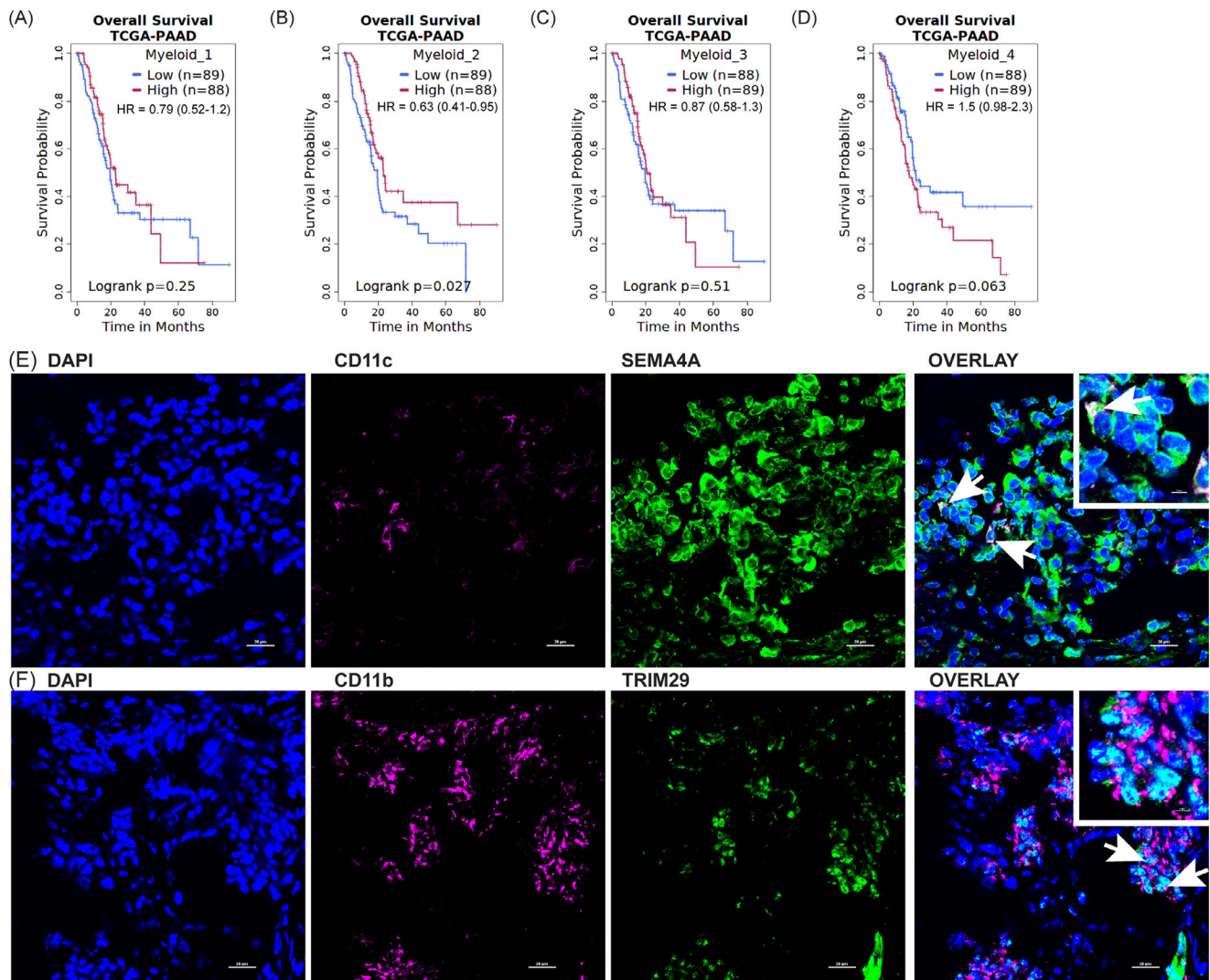


**FIGURE 6** Signature genes from myeloid subset predict overall survival in The Cancer Genome Atlas (TCGA)-pancreatic adenocarcinoma (PAAD) dataset. (A–D) Kaplan–Meier survival curve for ‘TCGA-PAAD’ patients sorted by overall expression of signature genes for each myeloid subcluster: recruited monocyte (A), dendritic cells (B), myeloid-derived suppressor cell (MDSC) (C) and tissue resident/epithelial-like macrophage (D). (E) Immunofluorescent (IF) staining for dendritic cell markers CD11c and SEMA4A in tumour 4. (F) IF staining for tissue resident/epithelial-like macrophage markers CD11b and TRIM29 in tumour 3. Images taken at 60× (20 μm scale). White arrows indicate co-stained cells. Inset indicates co-stained cells (5 μm scale).

function of these cells, *SEMA4A* and *TRIM29*, respectively, with known myeloid markers. *SEMA4A*, which improves the ability of dendritic cells to activate T-cell responses<sup>33,34</sup> and was elevated in our gene signatures for subcluster 2, was co-stained with CD11c, a dendritic cell marker (Figure 6E). *TRIM29* is implicated in the immunosuppressive functions of macrophages,<sup>96</sup> and we also identified *TRIM29*, which can function in the nucleoplasm,<sup>97</sup> expression in the nuclei of CD11b-expressing myeloid cells (Figure 6F). These data qualitatively validate the expression of *SEMA4A* and *TRIM29* with known myeloid cell markers, CD11c and CD11b, respectively. Taken together, these data indicate that snATAC-Seq analysis can provide signature genes of interest for myeloid cells, such as infil-

trating dendritic cells (myeloid subcluster 2) and tissue resident/epithelial-like macrophages (myeloid subcluster 4), which can be further explored in the preclinical and clinical settings.

## 4 | DISCUSSION

In this study, we demonstrate snATAC-Seq can determine the cell compositions of frozen benign pancreas and PDAC samples. Assaying the accessible chromatin regions provides rich information on regulome landscape including transcription factor activities and gene promoter openness. These data can be utilised to determine cell type

and infer molecular functionality. In PDAC specifically, previous studies have demonstrated that ATAC-Seq can be used to determine differentially accessible chromatin peaks in Epcam<sup>+</sup> epithelial cells sorted from surgically resected PDAC specimens. These peaks can then be used to predict patient disease-free survival.<sup>98</sup> Another study utilising scATAC-Seq from freshly acquired benign pancreatic, normal adjacent tissue and PDAC specimens demonstrated that the KRAS mutation locks open an enhancer network in human PDAC that is similar to that found in murine PDAC models.<sup>20</sup> Furthermore, another technique to look at open chromatin regions (single cell COOL-seq) has been used in PDAC specimens to demonstrate specific transcription factor binding motifs that may be important in pancreatic cancer progression.<sup>7</sup> To add to this body of literature, we employed snATAC-Seq to explore the intricate regulome landscape of the diverse myeloid populations present in PDAC tumours.

We demonstrated the composition differences among cell populations presented in benign pancreata and PDAC and validated our cell type annotations with snMultiomics and previously published scATAC-Seq,<sup>20</sup> adding rigour to our approach. snATAC-Seq was also used to compare the function of the benign pancreas, related to the pancreatic connection to the autonomic nervous system,<sup>56</sup> to the function of the cells in the PDAC tumour, which is related to infiltration of inflammatory cells similar to previous reports.<sup>15</sup> Our GO enrichment determined the function of individual cell populations with support from the literature: the acinar and endocrine cells had links to the nervous system,<sup>1,56</sup> due to their functions related to neuron projection. The fibroblasts were shown to regulate cell morphogenesis such as previous studies showing fibroblasts drive EMT in PDAC tumour cells.<sup>73</sup> We similarly identified functions of myeloid subsets, including immune response activation and regulation of lymphocyte and leukocyte activation. These findings were counter to previous studies showing myeloid subsets are primarily immunosuppressive in PDAC,<sup>2,11,79</sup> prompting further inquiry.

While the current study used four patient tumour samples to characterise myeloid subpopulations, the limited number of patients precluded associations with prognosis. Therefore, we used the determined gene signatures within a larger dataset to determine the influence of the ATAC defined unique populations in the myeloid compartment on survival. Unlike previous studies of infiltrating monocytes, we saw no correlation to overall survival based on expression of signature genes from monocyte<sup>2</sup> or MDSC<sup>79</sup> subclusters. Importantly, the previous studies measured monocytes<sup>2</sup> and MDSCs<sup>79</sup> in circulation, which may explain the differences in findings. The gene signature for dendritic cells predicted better overall sur-

vival, similar to previous reports for circulating dendritic cells.<sup>36</sup> Previous studies also show infiltrating dendritic cells promote a T cell response in PDAC,<sup>99</sup> and our gene signature showed expression of *SEMA4A*, which promotes T-cell activation.<sup>33,34</sup> Furthermore, there was a trend towards worse overall survival in patients with a tissue resident/epithelial-like macrophages gene signature, supporting studies showing TRMs responsible for PDAC progression in murine models<sup>5</sup> and chemotherapy resistance.<sup>43</sup> Similar to previous studies,<sup>5,11</sup> the tissue resident/epithelial-like signature had higher collagen expression. We also uniquely demonstrated *TRIM29* expression in the tissue resident/epithelial-like signature, which can drive macrophage immunosuppressive features.<sup>96</sup> The TRM/epithelial-like population was also like the epithelial-like macrophage population shown by scRNA-Seq of PDAC,<sup>11</sup> suggesting that TRMs and epithelial-like macrophages may arise from a similar cell population in PDAC tumours. The diverse populations of myeloid cells shown in this study are similar to scRNA-Seq studies showing unique populations within the myeloid cluster.<sup>11</sup>

Clinical trials focused on taming myeloid cells in PDAC have only been modestly successful. CCR2 antagonism therapy, which prohibits recruitment of circulating monocytes into the tumour, improved tumour control based on RECIST criteria when combined with standard of care FOLFIRINOX.<sup>3</sup> However, combining CCR2 antagonism with gemcitabine/nab-paclitaxel did not improve outcomes and was countered by risk of lung toxicity.<sup>4</sup> While the CCR2/CCL2 axis may recruit myeloid cells that are hijacked by the tumour to become immunosuppressive,<sup>2,3</sup> these cells can promote an anti-tumour response when activated to a pro-inflammatory state.<sup>95</sup> Furthermore, studies in murine models have shown TRMs, not monocytes, are the problematic population in PDAC,<sup>5</sup> but these cells have not been targeted clinically. Additional clinical trials have utilised CD40 agonism to promote antigen presenting cells to stimulate a T cell response,<sup>100</sup> again with limited efficacy. This may be in part due to dendritic cells also having an immunosuppressive function in tumours by expressing cytotoxic T lymphocyte-associated protein 4 (CTLA-4)<sup>101</sup> or programmed cell death protein 1 (PD-1),<sup>102</sup> preventing antigen presentation and T cell activation. Thus, while dendritic cells are critical for T cell activation,<sup>99,37</sup> overactivation can be detrimental and cause immunosuppression.<sup>37,101,102</sup> Such observations point to the heterogenous nature of the myeloid cell infiltrate in PDAC, which we demonstrate here. This heterogeneity is driven by the interplay between the many factors comprising the PDAC TME, such as tumour cells, stromal cells, immune cells and soluble factors, which can differently impact myeloid populations. For example, *CSF1-CSF1R*

interactions between tumour cells and macrophages,<sup>12</sup> respectively, are important for activation of macrophages. Importantly, colony stimulating factor 1 (CSF1) has been shown to be important for maintaining TRM populations in PDAC, which are pro-fibrotic and pro-tumour,<sup>5</sup> and may be responsible for therapeutic resistance to standard of care chemotherapy gemcitabine.<sup>43</sup> PDAC tumour cells can also inhibit development of dendritic cells by release of granulocyte colony stimulating factor (G-CSF), which inhibits IRF8-mediated development of dendritic cells in the bone marrow.<sup>36</sup> Furthermore, pancreatic stellate cells from the PDAC TME drive infiltrating myeloid cells towards a MDSC state via STAT3 signalling, which can in turn inhibit T-cell function.<sup>103</sup> In contrast, the combination of C-C motif chemokine ligand 2 (CCL2) and interferon gamma (IFN-g) can drive an anti-tumour phenotype in PDAC myeloid cells, and this is particularly important in the presence of CD40 agonist treatment.<sup>95</sup> Thus, technologies such as snATAC-Seq can be useful for understanding the presence and function of myeloid cell subpopulations, which we have shown in the present manuscript. Such an understanding could lead to a more targeted approach towards implementation of myeloid therapies rather than a 'copy/paste' or 'one size fits all' approach, which has failed to translate immunotherapies that have been successful in other cancers to PDAC.<sup>104</sup> Further studies utilising snATAC-Seq may uncover additional myeloid targets for future preclinical and clinical studies, emphasising a bedside to bench to bedside approach.

The current study has several potential limitations. While the current manuscript offers methodology for analysing myeloid populations in PDAC tumour specimens across multiple institutions with diverse patient demographics and treatment regimens, the current study only utilises four patients with benign pancreatic pathologies and four patients with PDAC. Given the limited number of PDAC patients, additional studies are warranted to better understand the myeloid populations, as this limited sample size may not be sufficient to conclusively characterise all potential myeloid subpopulations and their functions given tumour and patient heterogeneity. However, the present method provides a means for assaying frozen samples, which may broaden the available patient cohort by allowing for assessment of banked samples.

## 5 | CONCLUSION

Despite a small sample size used in our analysis, this manuscript demonstrates the strength of utilising frozen tumour samples with snATAC-Seq. Frozen samples can be used to study patients with known outcomes and

treatment conditions to tease apart the intricacies of the PDAC TME, particularly the myeloid subset, which can be challenging to study given the plasticity of the cells. Additional studies are warranted to understand how neoadjuvant therapies can affect myeloid subpopulations and how those myeloid subpopulations may in turn affect therapy response. With the implementation of such studies, patient-specific myeloid targets could be identified to better utilise myeloid therapies in particular patient populations or to implement novel myeloid targets.

## AUTHOR CONTRIBUTIONS

*Conceptualisation:* Hillary G. Pratt, Barbara Szomolay, Thomas Whalley, Sascha Ott, Brian A. Boone and Timothy D. Eubank. *Methodology:* Hillary G. Pratt, Sebastian A. Dziadowicz and Li Ma. *Assays:* Hillary G. Pratt and Sebastian A. Dziadowicz. *Data analysis:* Li Ma, Gangqing Hu, Barbara Szomolay and Thomas Whalley. *Writing:* Hillary G. Pratt, Li Ma and Gangqing Hu. *Supervision:* Brian A. Boone, Timothy D. Eubank and Gangqing Hu.

## ACKNOWLEDGEMENTS

Research reported in this publication was supported by the NIGMS 5U54GM104942-04 and NIGMS CoBRE award (5P20GM121322) (B.A.B.); NCI R01CA194013 and NCI R01CA192064 (T.D.E.); NIGMS P20 GM103434, U54 GM-104942 and P20 GM121322 (G.H.); and NIGMS T32 GM133369 (H.G.P.). Experiments were performed in the West Virginia University Flow Cytometry & Single Cell Core Facility, which is supported by the Institutional Development Awards (IDeA) from the National Institute of General Medical Sciences of the National Institutes of Health (NIH) under grant numbers U54GM104942 (CTR), P20GM121322 (TME CoBRE) and P20GM103434 (WV-INBRE). Genomics experiments were performed the West Virginia University Genomics Core Facility, which has been supported by NIH grant U54GM104942 and NSF MRI award 2117043. Sequencing was performed by the Marshall University Genomics Core and Bioinformatics Core and supported by the WV-INBRE grant (P20GM103434), the COBRE ACCORD grant (1P20GM121299) and the West Virginia Clinical and Translational Science Institute grant (2U54GM104942). Imaging experiments were performed in the West Virginia University Microscope Imaging Facility, which has been supported by the WVU Cancer Institute, the WVU HSC Office of Research and Graduate Education and NIH grants P20GM121322 and P20GM144230. The Nikon A1R/SIM used was supported by U54GM104942 and P20GM103434 and the analysis software was supported by P20GM103434. The content is solely the responsibility of the authors and does not necessarily represent the official views of the NIH.

## CONFLICT OF INTEREST STATEMENT

The authors declare they have no conflicts of interest.

## DATA AVAILABILITY STATEMENT

All raw sequenced data are publicly available at Gene Expression Omnibus under accession number GSE241896.

## ETHICS STATEMENT

Ethics was reviewed by Institutional Review Board and approval was obtained from West Virginia University (#1903496995), and all patients signed informed consent.

## ORCID

Brian A. Boone  <https://orcid.org/0000-0001-9006-059X>

## REFERENCES

- Fan J-Q, Wang M-F, Chen H-L, Shang D, Das J-K, Song J. Current advances and outlooks in immunotherapy for pancreatic ductal adenocarcinoma. *Mol Cancer*. 2020;19(1):32. doi:10.1186/s12943-020-01151-3
- Sanford DE, Belt BA, Panni RZ, et al. Inflammatory monocyte mobilization decreases patient survival in pancreatic cancer: a role for targeting the CCL2/CCR2 axis. *Clin Cancer Res*. 2013;19(13):3404-3415. doi:10.1158/1078-0432.CCR-13-0525
- Nywenning TM, Wang-Gillam A, Sanford DE, et al. Targeting tumour-associated macrophages with CCR2 inhibition in combination with FOLFIRINOX in patients with borderline resectable and locally advanced pancreatic cancer: a single-centre, open-label, dose-finding, non-randomised, phase 1b trial. *Lancet Oncol*. 2016;17(5):651-662. doi:10.1016/S1470-2045(16)00078-4
- Noel M, O'Reilly EM, Wolpin BM, et al. Phase 1b study of a small molecule antagonist of human chemokine (C-C motif) receptor 2 (PF-04136309) in combination with nab-paclitaxel/gemcitabine in first-line treatment of metastatic pancreatic ductal adenocarcinoma. *Invest New Drugs*. 2020;38(3):800-811. doi:10.1007/s10637-019-00830-3
- Zhu Y, Herndon JM, Sojka DK, et al. Tissue-resident macrophages in pancreatic ductal adenocarcinoma originate from embryonic hematopoiesis and promote tumor progression. *Immunity*. 2017;47(2):323-338.e6. doi:10.1016/j.immuni.2017.07.014
- Laviron M, Boissonnas A. Ontogeny of tumor-associated macrophages. *Front Immunol*. 2019;10:1799. doi:10.3389/fimmu.2019.01799
- Fan X, Lu P, Wang H, et al. Integrated single-cell multi-omics analysis reveals novel candidate markers for prognosis in human pancreatic ductal adenocarcinoma. *Cell Discov*. 2022;8(1):13. doi:10.1038/s41421-021-00366-y
- Chen K, Wang Q, Li M, et al. Single-cell RNA-seq reveals dynamic change in tumor microenvironment during pancreatic ductal adenocarcinoma malignant progression. *EBioMedicine*. 2021;66:103315. doi:10.1016/j.ebiom.2021.103315
- Li J, Byrne KT, Yan F, et al. Tumor cell-intrinsic factors underlie heterogeneity of immune cell infiltration and response to immunotherapy. *Immunity*. 2018;49(1):178-193.e7. doi:10.1016/j.immuni.2018.06.006
- Zhang D, Wu S, Pan S, et al. Single-cell sequencing reveals heterogeneity between pancreatic adenosquamous carcinoma and pancreatic ductal adenocarcinoma with prognostic value. *Front Immunol*. 2022;13:972298. doi:10.3389/fimmu.2022.972298
- Werba G, Weissinger D, Kawaler EA, et al. Single-cell RNA sequencing reveals the effects of chemotherapy on human pancreatic adenocarcinoma and its tumor microenvironment. *Nat Commun*. 2023;14(1):797. doi:10.1038/s41467-023-36296-4
- Yang K, Yang T, Yu J, Li F, Zhao X. Integrated transcriptional analysis reveals macrophage heterogeneity and macrophage-tumor cell interactions in the progression of pancreatic ductal adenocarcinoma. *BMC Cancer*. 2023;23(1):199. doi:10.1186/s12885-023-10675-y
- Jacobetz MA, Chan DS, Neesse A, et al. Hyaluronan impairs vascular function and drug delivery in a mouse model of pancreatic cancer. *Gut*. 2013;62(1):112-120. doi:10.1136/gutjnl-2012-302529
- Lin W, Noel P, Borazanci EH, et al. Single-cell transcriptome analysis of tumor and stromal compartments of pancreatic ductal adenocarcinoma primary tumors and metastatic lesions. *Genome Med*. 2020;12(1):80. doi:10.1186/s13073-020-00776-9
- Peng J, Sun BF, Chen CY, et al. Single-cell RNA-seq highlights intra-tumoral heterogeneity and malignant progression in pancreatic ductal adenocarcinoma. *Cell Res*. 2019;29(9):725-738. doi:10.1038/s41422-019-0195-y
- Pan Y, Lu F, Fei Q, et al. Single-cell RNA sequencing reveals compartmental remodeling of tumor-infiltrating immune cells induced by anti-CD47 targeting in pancreatic cancer. *J Hematol Oncol J Hematol Oncol*. 2019;12(1):124. doi:10.1186/s13045-019-0822-6
- Buenrostro JD, Wu B, Chang HY, Greenleaf WJ. ATAC-seq: a method for assaying chromatin accessibility genome-wide. *Curr Protoc Mol Biol*. 2015;109(1). doi:10.1002/0471142727.mb2129s109
- Corces MR, Trevino A, Hamilton EG, et al. Omni-ATAC-seq: improved ATAC-seq protocol. *Protoc Exch*. 2017. doi:10.1038/protex.2017.096
- Lavin Y, Winter D, Blecher-Gonen R, et al. Tissue-resident macrophage enhancer landscapes are shaped by the local microenvironment. *Cell*. 2014;159(6):1312-1326. doi:10.1016/j.cell.2014.11.018
- Li Y, He Y, Peng J, et al. Mutant Kras co-opts a proto-oncogenic enhancer network in inflammation-induced metastatic progenitor cells to initiate pancreatic cancer. *Nat Cancer*. 2020;2(1):49-65. doi:10.1038/s43018-020-00134-z
- Hao Y, Hao S, Andersen-Nissen E, et al. Integrated analysis of multimodal single-cell data. *Cell*. 2021;184(13):3573-3587.e29. doi:10.1016/j.cell.2021.04.048
- Stuart T, Srivastava A, Madad S, Lareau CA, Satija R. Single-cell chromatin state analysis with Signac. *Nat Methods*. 2021;18(11):1333-1341. doi:10.1038/s41592-021-01282-5
- Korsunsky I, Millard N, Fan J, et al. Fast, sensitive and accurate integration of single-cell data with harmony. *Nat Methods*. 2019;16(12):1289-1296. doi:10.1038/s41592-019-0619-0
- Waltman L, Van Eck NJ. A smart local moving algorithm for large-scale modularity-based community detection. *Eur Phys J B*. 2013;86(11):471. doi:10.1140/epjb/e2013-40829-0
- Rygiel AM, Unger LS, Sörgel FL, et al. Variants in the pancreatic CUB and zona pellucida-like domains 1 (CUZD1) gene in

- early-onset chronic pancreatitis—a possible new susceptibility gene. *Pancreatology*. 2022;22(5):564-571. doi:10.1016/j.pan.2022.04.015
26. Prévot PP, Simion A, Grimont A, et al. Role of the ductal transcription factors HNF6 and Sox9 in pancreatic acinar-to-ductal metaplasia. *Gut*. 2012;61(12):1723-1732. doi:10.1136/gutjnl-2011-300266
  27. Buckle A, Nozawa R-S, Kleinjan DA, Gilbert N. Functional characteristics of novel pancreatic Pax6 regulatory elements. *Hum Mol Genet*. 2018;27(19):3434-3448. doi:10.1093/hmg/ddy255
  28. Katsuta E, Qi Q, Peng X, Hochwald SN, Yan L, Takabe K. Pancreatic adenocarcinomas with mature blood vessels have better overall survival. *Sci Rep*. 2019;9(1):1310. doi:10.1038/s41598-018-37909-5
  29. Elyada E, Bolisetty M, Laise P, et al. Cross-species single-cell analysis of pancreatic ductal adenocarcinoma reveals antigen-presenting cancer-associated fibroblasts. *Cancer Discov*. 2019;9(8):1102-1123. doi:10.1158/2159-8290.CD-19-0094
  30. Bayne LJ, Beatty GL, Jhala N, et al. Tumor-derived granulocyte-macrophage colony-stimulating factor regulates myeloid inflammation and T cell immunity in pancreatic cancer. *Cancer Cell*. 2012;21(6):822-835. doi:10.1016/j.ccr.2012.04.025
  31. Poirier SJ, Boudreau LH, Flamand N, Surette ME. LPS induces ALOX5 promoter activation and 5-lipoxygenase expression in human monocytic cells. *Prostaglandins Leukot Essent Fatty Acids*. 2020;154:102078. doi:10.1016/j.plefa.2020.102078
  32. Awad F, Assrawi E, Jumeau C. Impact of human monocyte and macrophage polarization on NLR expression and NLRP3 inflammasome activation. *PLoS One*. 2017;12(4):e0175336. doi:10.1371/journal.pone.0175336
  33. Kumanogoh A, Marukawa S, Suzuki K, et al. Class IV semaphorin Sema4A enhances T-cell activation and interacts with Tim-2. *Nature*. 2002;419(6907):629-633. doi:10.1038/nature01037
  34. Lu N, Li Y, Zhang Z, et al. Human Semaphorin-4A drives Th2 responses by binding to receptor ILT-4. *Nat Commun*. 2018;9(1):742. doi:10.1038/s41467-018-03128-9
  35. van Rijn A, Paulis L, te Riet J, et al. Semaphorin 7A promotes chemokine-driven dendritic cell migration. *J Immunol*. 2016;196(1):459-468.
  36. Meyer MA, Baer JM, Knolhoff BL, et al. Breast and pancreatic cancer interrupt IRF8-dependent dendritic cell development to overcome immune surveillance. *Nat Commun*. 2018;9(1):1250. doi:10.1038/s41467-018-03600-6
  37. Neophytou CM, Pierides C, Christodoulou MI, Costeas P, Kyriakou TC, Papageorgis P. The role of tumor-associated myeloid cells in modulating cancer therapy. *Front Oncol*. 2020;10:899. doi:10.3389/fonc.2020.00899
  38. Gabrilovich DI, Nagaraj S. Myeloid-derived suppressor cells as regulators of the immune system. *Nat Rev Immunol*. 2009;9(3):162-174. doi:10.1038/nri2506
  39. Schep AN, Wu B, Buenrostro JD, Greenleaf WJ. chromVAR: inferring transcription-factor-associated accessibility from single-cell epigenomic data. *Nat Methods*. 2017;14(10):975-978. doi:10.1038/nmeth.4401
  40. Zhou Y, Zhou B, Pache L, et al. Metascape provides a biologist-oriented resource for the analysis of systems-level datasets. *Nat Commun*. 2019;10(1):1523. doi:10.1038/s41467-019-09234-6
  41. Dwivedi B, Mumme H, Satpathy S, Bhasin SS, Bhasin M, Survival Genie, a web platform for survival analysis across pediatric and adult cancers. *Sci Rep*. 2022;12(1):3069. doi:10.1038/s41598-022-06841-0
  42. Sun K, Mylavarapu C, Crenshaw A, et al. Pancreatic head vs pancreatic body/tail cancer: are they different? *World J Gastrointest Oncol*. 2022;14(3):716-723. doi:10.4251/wjgo.v14.i3.716
  43. Zhang J, Song J, Tang S, et al. Multi-omics analysis reveals the chemoresistance mechanism of proliferating tissue-resident macrophages in PDAC via metabolic adaptation. *Cell Rep*. 2023;42(6):112620. doi:10.1016/j.celrep.2023.112620
  44. Williams JA. Regulation of normal and adaptive pancreatic growth. Pancrepedia: Exocrine Pancreas Knowledge Base. American Pancreatic Association. doi:10.3998/panc.2020.05
  45. Hoang CQ, Hale MA, Azevedo-Pouly AC, et al. Transcriptional maintenance of pancreatic acinar identity, differentiation, and homeostasis by PTF1A. *Mol Cell Biol*. 2016;36(24):3033-3047. doi:10.1128/MCB.00358-16
  46. Cebola I, Rodríguez-Seguí SA, Cho CHH, et al. TEAD and YAP regulate the enhancer network of human embryonic pancreatic progenitors. *Nat Cell Biol*. 2015;17(5):615-626. doi:10.1038/ncb3160
  47. Eferl R, Wagner EF. AP-1: a double-edged sword in tumorigenesis. *Nat Rev Cancer*. 2003;3(11):859-868. doi:10.1038/nrc1209
  48. Park J, Eisenbarth D, Choi W, et al. YAP and AP-1 cooperate to initiate pancreatic cancer development from ductal cells in mice. doi:10.1158/0008-5472.CAN-20-0907
  49. Wortham M, Sander M. Transcriptional mechanisms of pancreatic  $\beta$ -cell maturation and functional adaptation. *Trends Endocrinol Metab*. 2021;32(7):474-487. doi:10.1016/j.tem.2021.04.011
  50. De Val S, Black BL. Transcriptional control of endothelial cell development. *Dev Cell*. 2009;16(2):180-195. doi:10.1016/j.devcel.2009.01.014
  51. Wei L, Lin Q, Lu Y, et al. Cancer-associated fibroblasts-mediated ATF4 expression promotes malignancy and gemcitabine resistance in pancreatic cancer via the TGF- $\beta$ 1/SMAD2/3 pathway and ABCC1 transactivation. *Cell Death Dis*. 2021;12(4):334. doi:10.1038/s41419-021-03574-2
  52. Bhat NK, Thompson CB, Lindsten T, et al. Reciprocal expression of human ETS1 and ETS2 genes during T-cell activation: regulatory role for the protooncogene ETS1. *Proc Natl Acad Sci U S A*. 1990;87(10):3723-3727. doi:10.1073/pnas.87.10.3723
  53. Friedman AD. C/EBP $\alpha$  induces PU.1 and interacts with AP-1 and NF- $\kappa$ B to regulate myeloid development. *Blood Cells Mol Dis*. 2007;39(3):340-343. doi:10.1016/j.bcmd.2007.06.010
  54. Song H, Dong M, Zhou J, Sheng W, Li X, Gao W. Expression and prognostic significance of TRPV6 in the development and progression of pancreatic cancer. *Oncol Rep*. 2018;39(3):1432-1440. doi:10.3892/or.2018.6216
  55. Wang H, Chen L, Qi L, et al. A single-cell atlas of tumor-infiltrating immune cells in pancreatic ductal adenocarcinoma. *Mol Cell Proteomics*. 2022;21(8):100258. doi:10.1016/j.mcpro.2022.100258

56. Lkhagvasuren B, Mee-Inta O, Zhao ZW, Hiramoto T, Boldbaatar D, Kuo YM. Pancreas–brain crosstalk. *Front Neuroanat.* 2021;15:691777. doi:10.3389/fnana.2021.691777
57. Pollard TD, Cooper JA. Actin, a central player in cell shape and movement. *Science.* 2009;326(5957):1208-1212. doi:10.1126/science.1175862
58. Qu X, Nyeng P, Xiao F, Dorantes J, Jensen J. Growth factor independence-1 (Gfi1) is required for pancreatic acinar unit formation and centroacinar cell differentiation. *Cell Mol Gastroenterol Hepatol.* 2015;1(2):233-247.e1. doi:10.1016/j.jcmgh.2014.12.004
59. Patzek S, Liu Z, De La OS, et al. Loss of Fgf9 in mice leads to pancreatic hypoplasia and asplenia. *iScience.* 2023;26(4):106500. doi:10.1016/j.isci.2023.106500
60. Guillemot F, Zimmer C. From cradle to grave: the multiple roles of fibroblast growth factors in neural development. *Neuron.* 2011;71(4):574-588. doi:10.1016/j.neuron.2011.08.002
61. Zhang X, Huang CT, Chen J, et al. Pax6 is a human neuroectoderm cell fate determinant. *Cell Stem Cell.* 2010;7(1):90-100. doi:10.1016/j.stem.2010.04.017
62. Ediger BN, Du A, Liu J, et al. Islet-1 is essential for pancreatic B-cell function. 2014;63.
63. Tixi W, Maldonado M, Chang YT, et al. Coordination between ECM and cell-cell adhesion regulates the development of islet aggregation, architecture, and functional maturation. *eLife.* 2023;12:e90006. doi:10.7554/eLife.90006
64. Rashid M, Olson EC. Delayed cortical development in mice with a neural specific deletion of  $\beta 1$  integrin. *Front Neurosci.* 2023;17:1158419. doi:10.3389/fnins.2023.1158419
65. Du X, Yi X, Zou X, et al. PCDH1, a poor prognostic biomarker and potential target for pancreatic adenocarcinoma metastatic therapy. *BMC Cancer.* 2023;23(1):1102. doi:10.1186/s12885-023-11474-1
66. Ye Z, Yang Y, Wei Y, Li L, Wang X, Zhang J. PCDH1 promotes progression of pancreatic ductal adenocarcinoma via activation of NF- $\kappa$ B signalling by interacting with KPNB1. *Cell Death Dis.* 2022;13(7):633. doi:10.1038/s41419-022-05087-y
67. Tsuji S, Washimi K, Kageyama T, et al. HEG1 is a novel mucin-like membrane protein that serves as a diagnostic and therapeutic target for malignant mesothelioma. *Sci Rep.* 2017;7(1):45768. doi:10.1038/srep45768
68. Long Y, Wu J, Shen Y, et al. CAPG is a novel biomarker for early gastric cancer and is involved in the Wnt/ $\beta$ -catenin signaling pathway. *Cell Death Discov.* 2024;10(1):15. doi:10.1038/s41420-023-01767-6
69. Xiang X, Wang Y, Zhang H, et al. Vasodilator-stimulated phosphoprotein promotes liver metastasis of gastrointestinal cancer by activating a  $\beta 1$ -integrin-FAK-YAP1/TAZ signaling pathway. *Npj Precis Oncol.* 2018;2(1):2. doi:10.1038/s41698-017-0045-7
70. Fukumura D, Gohongi T, Kadambi A, et al. Predominant role of endothelial nitric oxide synthase in vascular endothelial growth factor-induced angiogenesis and vascular permeability. *Proc Natl Acad Sci U S A.* 2001;98(5):2604-2609. doi:10.1073/pnas.041359198
71. Lampson BL, Kendall SD, Ancrile BB, et al. Targeting eNOS in pancreatic cancer. *Cancer Res.* 2012;72(17):4472-4482. doi:10.1158/0008-5472.CAN-12-0057
72. Murakami M, Nguyen LT, Zhang ZW, et al. The FGF system has a key role in regulating vascular integrity. *J Clin Invest.* 2008;118(10):3355-3366. doi:10.1172/JCI35298
73. Bulle A, Lim KH. Beyond just a tight fortress: contribution of stroma to epithelial-mesenchymal transition in pancreatic cancer. *Signal Transduct Target Ther.* 2020;5(1):249. doi:10.1038/s41392-020-00341-1
74. Alcaraz LB, Mallavialle A, Mollevi C, et al. SPARC in cancer-associated fibroblasts is an independent poor prognostic factor in non-metastatic triple-negative breast cancer and exhibits pro-tumor activity. *Int J Cancer.* 2023;152(6):1243-1258. doi:10.1002/ijc.34345
75. Shah K, Al-Haidari A, Sun J, Kazi JU. T cell receptor (TCR) signaling in health and disease. *Signal Transduct Target Ther.* 2021;6(1):412. doi:10.1038/s41392-021-00823-w
76. Liu S, Zhou B, Wu L, Sun Y, Chen J, Liu S. Single-cell differential splicing analysis reveals high heterogeneity of liver tumor-infiltrating T cells. *Sci Rep.* 2021;11(1):5325. doi:10.1038/s41598-021-84693-w
77. Schroder K, Tschopp J. The inflammasomes. *Cell.* 2010;140(6):821-832. doi:10.1016/j.cell.2010.01.040
78. Daley D, Mani VR, Mohan N, et al. NLRP3 signaling drives macrophage-induced adaptive immune suppression in pancreatic carcinoma. *J Exp Med.* 2017;214(6):1711-1724. doi:10.1084/jem.20161707
79. Trovato R, Fiore A, Sartori S, et al. Immunosuppression by monocytic myeloid-derived suppressor cells in patients with pancreatic ductal carcinoma is orchestrated by STAT3. *J Immunother Cancer.* 2019;7(1):255. doi:10.1186/s40425-019-0734-6
80. Von Moltke J, Trinidad NJ, Moayeri M, et al. Rapid induction of inflammatory lipid mediators by the inflammasome in vivo. *Nature.* 2012;490(7418):107-111. doi:10.1038/nature11351
81. Menon V, Ghaffari S. Transcription factors FOXO in the regulation of homeostatic hematopoiesis. *Curr Opin Hematol.* 2018;25(4):290-298. doi:10.1097/MOH.0000000000000441
82. Brykczynska U, Geigges M, Wiedemann SJ, et al. Distinct transcriptional responses across tissue-resident macrophages to short-term and long-term metabolic challenge. *Cell Rep.* 2020;30(5):1627-1643.e7. doi:10.1016/j.celrep.2020.01.005
83. Calderon B, Carrero JA, Ferris ST, et al. The pancreas anatomy conditions the origin and properties of resident macrophages. *J Exp Med.* 2015;212(10):1497-1512. doi:10.1084/jem.20150496
84. Ghislat G, Cheema AS, Baudoin E, et al. NF- $\kappa$ B-dependent IRF1 activation programs cDC1 dendritic cells to drive antitumor immunity. *Sci Immunol.* 2021;6(61):eabg3570. doi:10.1126/sciimmunol.abg3570
85. Tailor P, Tamura T, Ozato K. IRF family proteins and type I interferon induction in dendritic cells. *Cell Res.* 2006;16(2):134-140. doi:10.1038/sj.cr.7310018
86. Kurotaki D, Nakabayashi J, Nishiyama A, et al. Transcription factor IRF8 governs enhancer landscape dynamics in mononuclear phagocyte progenitors. *Cell Rep.* 2018;22(10):2628-2641. doi:10.1016/j.celrep.2018.02.048
87. Alam Z, Devalaraja S, Li M, et al. Counter regulation of Spic by NF- $\kappa$ B and STAT signaling controls inflammation and iron metabolism in macrophages. *Cell Rep.* 2020;31(13):107825. doi:10.1016/j.celrep.2020.107825

88. Ma RY, Black A, Qian BZ. Macrophage diversity in cancer revisited in the era of single-cell omics. *Trends Immunol.* 2022;43(7):546-563. doi:10.1016/j.it.2022.04.008
89. Suzuki E, Williams S, Sato S, Gilkeson G, Watson DK, Zhang XK. The transcription factor Fli-1 regulates monocyte, macrophage and dendritic cell development in mice. *Immunology.* 2013;139(3):318-327. doi:10.1111/imm.12070
90. Fontana MF, Baccarella A, Pancholi N, Pufall MA, Herbert DR, Kim CC. JUNB is a key transcriptional modulator of macrophage activation. *J Immunol.* 2015;194(1):177-186. doi:10.4049/jimmunol.1401595
91. Alshetaiwi H, Pervolarakis N, McIntyre LL, et al. Defining the emergence of myeloid-derived suppressor cells in breast cancer using single-cell transcriptomics. *Sci Immunol.* 2020;5(44):eaay6017. doi:10.1126/sciimmunol.aay6017
92. Waight JD, Netherby C, Hensen ML, et al. Myeloid-derived suppressor cell development is regulated by a STAT/IRF-8 axis. *J Clin Invest.* 2013;123(10):4464-4478. doi:10.1172/JCI68189
93. Saclier M, Angelini G, Bonfanti C, Mura G, Temponi G, Messina G. Selective ablation of NFIX in macrophages attenuates muscular dystrophy by inhibiting fibro-adipogenic progenitor-dependent fibrosis. *J Pathol.* 2022;257(3):352-366. doi:10.1002/path.5895
94. Adiko AC, Babdor J, Gutiérrez-Martínez E, Guermontprez P, Saveanu L. Intracellular transport routes for MHC I and their relevance for antigen cross-presentation. *Front Immunol.* 2015;6:335. doi:10.3389/fimmu.2015.00335
95. Long KB, Gladney WL, Tooker GM, Graham K, Fraietta JA, Beatty GL. IFN $\gamma$  and CCL2 cooperate to redirect tumor-infiltrating monocytes to degrade fibrosis and enhance chemotherapy efficacy in pancreatic carcinoma. *Cancer Discov.* 2016;6(4):400-413. doi:10.1158/2159-8290.CD-15-1032
96. Xing J, Weng L, Yuan B, et al. Identification of a role for TRIM29 in the control of innate immunity in the respiratory tract. *Nat Immunol.* 2016;17(12):1373-1380. doi:10.1038/ni.3580
97. Masuda Y, Takahashi H, Sato S, et al. TRIM29 regulates the assembly of DNA repair proteins into damaged chromatin. *Nat Commun.* 2015;6(1):7299. doi:10.1038/ncomms8299
98. Dhara S, Chhangawala S, Chintalapudi H, et al. Pancreatic cancer prognosis is predicted by an ATAC-array technology for assessing chromatin accessibility. *Nat Commun.* 2021;12(1):3044. doi:10.1038/s41467-021-23237-2
99. Hegde S, Krisnawan VE, Herzog BH, et al. Dendritic cell paucity leads to dysfunctional immune surveillance in pancreatic cancer. *Cancer Cell.* 2020;37(3):289-307. doi:10.1016/j.ccell.2020.02.008
100. Byrne KT, Betts CB, Mick R, et al. Neoadjuvant selicrelumab, an agonist CD40 antibody, induces changes in the tumor microenvironment in patients with resectable pancreatic cancer. *Clin Cancer Res.* 2021;27(16):4574-4586. doi:10.1158/1078-0432.CCR-21-1047
101. Ghorbaninezhad F, Masoumi J, Bakhshivand M, et al. CTLA-4 silencing in dendritic cells loaded with colorectal cancer cell lysate improves autologous T cell responses in vitro. *Front Immunol.* 2022;13:931316. doi:10.3389/fimmu.2022.931316
102. Lim TS, Chew V, Sieow JL, et al. PD-1 expression on dendritic cells suppresses CD8<sup>+</sup> T cell function and antitumor immunity. *Oncol Immunology.* 2016;5(3):e1085146. doi:10.1080/2162402X.2015.1085146
103. Mace TA, Ameen Z, Collins A, et al. Pancreatic cancer-associated stellate cells promote differentiation of myeloid-derived suppressor cells in a STAT3-dependent manner. *Cancer Res.* 2013;73(10):3007-3018. doi:10.1158/0008-5472.CAN-12-4601
104. Hester R, Mazur PK, McAllister F. Immunotherapy in pancreatic adenocarcinoma: beyond “copy/paste”. *Clin Cancer Res.* 2021;27(23):6287-6297. doi:10.1158/1078-0432.CCR-18-0900

## SUPPORTING INFORMATION

Additional supporting information can be found online in the Supporting Information section at the end of this article.

**How to cite this article:** Pratt HG, Ma L, Dziadowicz SA, et al. Analysis of single nuclear chromatin accessibility reveals unique myeloid populations in human pancreatic ductal adenocarcinoma. *Clin Transl Med.* 2024;14:e1595. <https://doi.org/10.1002/ctm2.1595>